

Correlations enable lossless ergotropy transport

Rick P. A. Simon,^{1, 2,*} Janet Anders,^{1, 2, †} and Karen V. Hovhannisyan^{1, ‡}

¹University of Potsdam, Institute of Physics and Astronomy,
Karl-Liebknecht-Str. 24-25, 14476 Potsdam, Germany

²Department of Physics and Astronomy, University of Exeter, Stocker Road, Exeter EX4 4QL, UK

“A battery powers a device” can be read as “work stored in the battery is being transported to the device.” In quantum batteries, the total amount of stored work can be measured by ergotropy, which is the maximal work extractable by unitary operations. Transporting ergotropy is fundamentally different from transporting energy, and here we find that ergotropy can be *gained* even when the transmission channel is strictly energy conserving. We show that, generically, ergotropy transport is lossy whenever the two systems start uncorrelated. In contrast, for a large class of correlated initial states, transport can be gainful. Furthermore, a single correlated state can be used multiple times, allowing to transport without losses an order of magnitude more work than the battery capacity. Correlations are thus a useful resource for ergotropy transport, and we quantify how this resource is consumed during gainful transport.

Introduction.—Batteries store work, it is their sole function. By natural extension, any quantum system storing work can be called a quantum battery. By storing work we mean storing energy that is available to be extracted in the form of work. Many fundamental aspects of quantum batteries’ storage capacity [1–5], charging speed [6–10], and stability [11–21] have been studied [22]. However, the no less fundamental matter of transporting a given amount of “charge” (i.e., work) from the battery to a consumption unit without external energetic intervention has so far received little attention [4, 21, 23–25]. A quantum battery autonomously powering a (quantum) device is a paradigmatic example of this scenario.

The charge level of a quantum battery, i.e., the total amount of work stored in it, is standardly quantified by ergotropy [1–13, 16–31]. It is the maximal amount of work that can be extracted from a system *unitarily* [32]. However, a battery performing work on a consumption unit means that the two systems interact with each other. And when they are of comparable size, the process will generally not be unitary for either system. This makes the problem of ergotropy transport highly non-trivial: When will this nonunitarity cause losses during transport? And can nonunitarity be leveraged to facilitate the transport?

In this paper, we put forth a rigorous framework for autonomous ergotropy transport between two quantum systems. We establish that the efficiency of transport ultimately depends on the initial correlations between the battery and the consumption unit. If they start uncorrelated, ergotropy will generically be partially lost during transport. However, if they start correlated, the transport may even be gainful, i.e., the consumption unit may receive more ergotropy than the battery sends.

Ergotropy and its transport.—If H is the Hamiltonian of a system that lives in a d -dimensional Hilbert space,

and ρ is its state, then the ergotropy is [32]

$$\mathcal{E}(\rho) := \text{Tr}(\rho H) - \min_U \text{Tr}(U \rho U^\dagger H). \quad (1)$$

Here the minimization is over *all* unitary operations. By construction, the optimal unitary and ergotropy depend solely on ρ and H .

In this paper, we focus on the bipartite scenario of transporting ergotropy from system B (battery) to system C (consumption unit). To make the bookkeeping of energy and entropy as clean as possible, we choose the transport “channel” to be strictly energy conserving and unitary. Namely, the operation that acts on BC to perform the transport is unitary, call it U_{BC} , and strict energy conservation means [33–37]

$$[U_{BC}, H_{BC}] = 0, \quad (2)$$

where $\mathbb{0}$ is the zero operator and

$$H_{BC} = H_B \otimes \mathbb{1}_C + \mathbb{1}_B \otimes H_C \quad (3)$$

is the total Hamiltonian of BC before and after the transport (during the transport, the Hamiltonian is varied in time so as to generate U_{BC}). Here H_B and H_C are, respectively, the Hamiltonians of B and C and $\mathbb{1}$ is the identity operator. A schematic of this process is depicted in Fig. 1.

The local evolution on B and C induced by U_{BC} can be unitary only under very restrictive conditions [36, 38–40]. In general, the individual evolutions of B and C will be (highly) nonunitary. Because of this, ergotropy transport is fundamentally different from energy transport [41–46] as well as the process of increasing one system’s average energy at the expense of another system’s ergotropy [47, 48]. For example, when a thermal system is heated up, its energy increases, but its ergotropy remains zero. Conversely, it is possible to purify a system’s state without changing its energy, which means its ergotropy increases while its energy remains fixed.

The main figure of merit we consider is the quality of the transport. It is naturally characterized by how much

* risimon@uni-potsdam.de

† janet@qipc.org

‡ karen.hovhannisyan@uni-potsdam.de

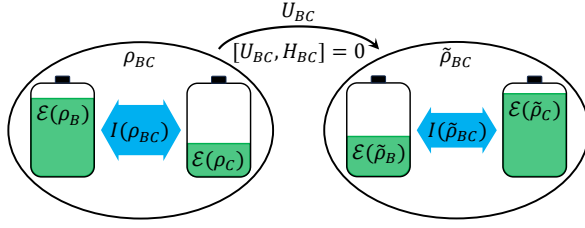


Figure 1. Schematic of transporting ergotropy from battery (B) to consumption unit (C). Initially, the systems do not interact, and their ergotropies are $\mathcal{E}(\rho_B)$ and $\mathcal{E}(\rho_C)$. Then an energy-conserving unitary U_{BC} transforms the initial joint state ρ_{BC} into $\tilde{\rho}_{BC}$, changing local ergotropies to $\mathcal{E}(\tilde{\rho}_B)$ and $\mathcal{E}(\tilde{\rho}_C)$. If C gains more ergotropy than B loses, then the transport is gainful. Otherwise, the transport is lossy. Our main objective is determining when the transport is gainful. One of our main results is that the amount of correlations between B and C , as quantified by the quantum mutual information I , is a key resource for achieving a gainful transport.

the channel adds to the ergotropy it transports. We call the added amount *ergotropy gain*. By definition, it is the difference between the amount of ergotropy lost by B and that received by C :

$$\mathcal{E}_G := \mathcal{E}(\tilde{\rho}_B) + \mathcal{E}(\tilde{\rho}_C) - \mathcal{E}(\rho_B) - \mathcal{E}(\rho_C), \quad (4)$$

where $\rho_B = \text{Tr}_C[\rho_{BC}]$ and $\rho_C = \text{Tr}_B[\rho_{BC}]$ are the marginals of the initial state of BC , ρ_{BC} . Similarly, $\tilde{\rho}_B$ and $\tilde{\rho}_C$ are the marginals of $\tilde{\rho}_{BC} = U_{BC}\rho_{BC}U_{BC}^\dagger$, which is the final, post-transport state of BC . When $\mathcal{E}_G < 0$, namely, when ergotropy is dissipated during transport, we say that the channel is lossy. When $\mathcal{E}_G \geq 0$, it is lossless, and gainful when $\mathcal{E}_G > 0$.

As Eq. (4) suggests, the ergotropy gain can also be interpreted as the difference between final and initial values of the “locally extractable ergotropy.” The latter is the maximal work extractable by unitary operations of the form $U_B \otimes U_C$, and is obviously equal to $\mathcal{E}(\rho_B) + \mathcal{E}(\rho_C)$. Here “local” refers to quantities pertaining to individual systems (B or C), to contrast with BC -wide (“global”) quantities. This observation allows us to connect the ergotropy gain to the so-called “ergotropic gap” [49], defined as the difference between the global and locally extractable ergotropies:

$$\delta_{BC}^\mathcal{E} := \mathcal{E}(\rho_{BC}) - \mathcal{E}(\rho_B) - \mathcal{E}(\rho_C) \geq 0. \quad (5)$$

The ergotropic gap, $\delta_{BC}^\mathcal{E}$, gives the amount of work hidden from local operations. Whenever B and C do not interact, i.e., the total Hamiltonian is of the form given by Eq. (3), $\delta_{BC}^\mathcal{E}$ depends only on the spectra of the global and local states. To see that, let us first invoke the well-known fact that the minimum in Eq. (1) is delivered by the unitary that rotates ρ to the so-called passive state ρ^\downarrow [32, 50, 51], and thus

$$\mathcal{E}(\rho) = \text{Tr}[(\rho - \rho^\downarrow)H]. \quad (6)$$

The passive state $\rho^\downarrow = \sum_k \lambda_k |E_k\rangle \langle E_k|$, where $|E_k\rangle$ are the eigenvectors of H for which the corresponding eigenvalues are ordered increasingly ($E_0 \leq \dots \leq E_{d-1}$) and $\lambda_0 \geq \dots \geq \lambda_{d-1} \geq 0$ are the eigenvalues of ρ in decreasing order [52]. Using Eq. (6), it is straightforward to show that

$$\delta_{BC}^\mathcal{E} = \text{Tr}[(\rho_B^\downarrow \otimes \rho_C^\downarrow - \rho_{BC}^\downarrow)H_{BC}], \quad (7)$$

where ρ_{BC}^\downarrow is passive with respect to H_{BC} and ρ_X^\downarrow is passive with respect to H_X ($X = B, C$).

Note that, as directly follows from the definition in Eq. (1), the action of an energy-conserving unitary on a state does not change its ergotropy. Hence, since U_{BC} is energy conserving, $\mathcal{E}(\tilde{\rho}_{BC}) = \mathcal{E}(\rho_{BC})$. Keeping this in mind, we can cast the ergotropy gain, as defined in Eq. (4), as a change in the ergotropic gap:

$$\mathcal{E}_G = \delta_{BC}^\mathcal{E} - \tilde{\delta}_{BC}^\mathcal{E}. \quad (8)$$

Thus, positive ergotropy gain is achieved when the energy-conserving unitary “redistributes” the ergotropy in the total system so that more of the global ergotropy becomes locally extractable. The resource expended for achieving the gain is the ergotropic gap. We emphasize that, in general, the transport unitary U_{BC} acts globally, and therefore $\tilde{\rho}_X$ is not reachable from ρ_X by local unitary evolutions.

A useful consequence of Eq. (8) and the fact that the ergotropic gap is a nonnegative quantity is the following lemma.

Lemma 1 (Lossy transport of ergotropy). *Ergotropy transport cannot be gainful, i.e., $\mathcal{E}_G \leq 0$, whenever $\delta_{BC}^\mathcal{E} = 0$.*

In other words, for gainful transport to be possible, the initial ergotropic gap must be positive. Importantly, the presence of a nonzero ergotropic gap is linked to the correlations in the system [2, 49, 53–55]. It can be used to witness entanglement [2, 53–55] or quantum discord [49]. In general, however, the relation between ergotropic gap and correlations is not exact: there exist uncorrelated states for which $\delta_{BC}^\mathcal{E} > 0$ and correlated states for which $\delta_{BC}^\mathcal{E} = 0$. The most prominent example of the former situation is the well-known phenomenon of activation, where two uncorrelated copies of a passive state ρ turn out non-passive (“active”) when considered jointly; i.e., $\rho \otimes \rho$ is active [50, 51].

Activation can happen only in Hilbert-space dimensions ≥ 3 . When each system is a qubit, all passive states are Gibbs states (i.e., are $\propto e^{-\beta H}$, $\beta > 0$), so no activation is possible [50, 51]. In fact, as the following lemma shows, the product of *any* two qubit states, $\rho_B \otimes \rho_C$, has strong limitations when it comes to ergotropy transport.

Lemma 2 (Two qubit case). *For two qubits, $\mathcal{E}_G \leq 0$ whenever the initial state is uncorrelated; i.e., $\rho_{BC} = \rho_B \otimes \rho_C$.*

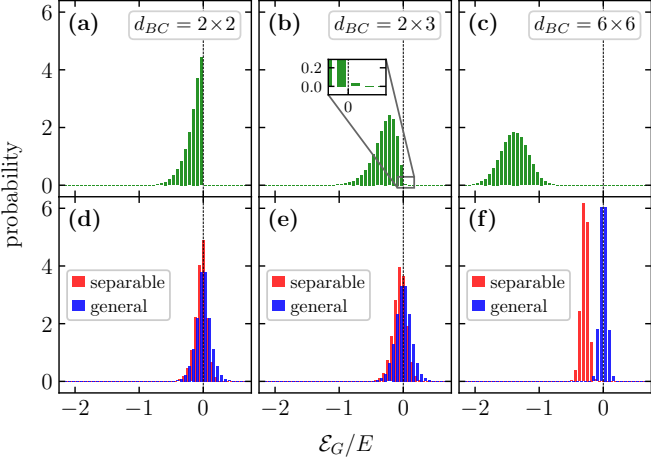


Figure 2. Distribution of ergotropy gain \mathcal{E}_G for randomly sampled initial states, Hamiltonians H_{BC} , and energy-conserving unitaries U_{BC} . In panels (a), (b), and (c), ρ_{BC} is a product of random ρ_B and ρ_C . The states are drawn from the Hilbert–Schmidt measure, H_{BC} are sampled from the Gaussian Unitary Ensemble, and U_{BC} are sampled from the Haar measure. Ergotropy gain follows a bell-shaped distribution, and its ensemble average, $\langle \mathcal{E}_G \rangle$, decreases as the Hilbert space dimension d_{BC} grows. Each of the panels (d), (e), and (f) shows two histograms of \mathcal{E}_G : one for separable and one for general states of BC (H_{BC} and U_{BC} sampled as above). These demonstrate that separable states perform almost as well as all states, implying that entanglement has no pronounced role in ergotropy transport. Each histogram depicts 10^6 points. The quantity E is a characteristic energy scale of the system. For qubits, E is the energy gap. In higher dimensions, defining a dimensionless Hamiltonian becomes nontrivial, and \mathcal{E}_G/E is just a shorthand notation for dimensionless ergotropy gain (see Appendix C for details).

This lemma is proven in Appendix A. Importantly, it does not imply ‘‘deterministic’’ relation between \mathcal{E}_G and correlations—the presence of correlations does not necessitate $\mathcal{E}_G > 0$. For example, the state $\frac{1}{2} |0_B 0_C\rangle \langle 0_B 0_C| + \frac{1}{2} |\Psi^+\rangle \langle \Psi^+|$, where $|\Psi^+\rangle = (|0_B 1_C\rangle + |1_B 0_C\rangle)/\sqrt{2}$ [56], is entangled but has zero ergotropic gap [57].

In Appendix B, we provide an alternative proof of Lemma 2 by making a connection to the so-called quantum marginal problem [58–60] and using its solution for two qubits [58]. In fact, we go even deeper and show that this connection can be useful in both ways, by deriving a family of nontrivial inequalities for quantum marginals *in arbitrary dimensions* from the simple fact that $\delta_{BC}^{\mathcal{E}} \geq 0$.

As mentioned above, an analog of Lemma 2 cannot hold in higher Hilbert-space dimensions. The minimal counterexample is found in 2×3 dimensions. Take B and C with Hamiltonians $H_B = E |1\rangle_B \langle 1|$ and $H_C = E |1\rangle_C \langle 1| + E |2\rangle_C \langle 2|$. Then, $\rho_B \otimes \rho_C$, with $\rho_B = \frac{1}{2} \mathbb{1}_B$ and $\rho_C = \frac{1}{2} |0\rangle_C \langle 0| + \frac{1}{2} |1\rangle_C \langle 1|$, is not passive despite both ρ_B and ρ_C being passive.

However, as our extensive numerics show, even in higher dimensions correlations play a central role when

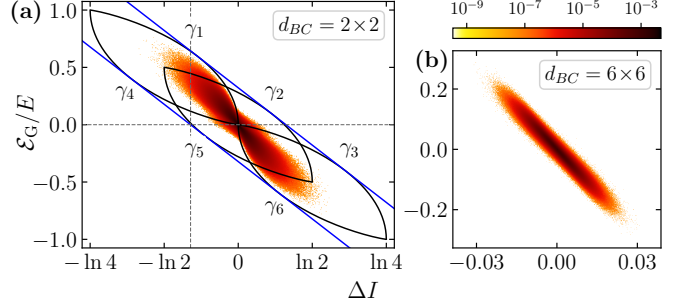


Figure 3. 2D histogram of \mathcal{E}_G vs ΔI for general ρ_{BC} , H_{BC} , and U_{BC} randomly generated as in Fig. 2. Panel (a) is for ergotropy transport between two qubits. Here the points distribute along $\mathcal{E}_G/E = -\Delta I/\ln 4$, within the strip laying between the two blue lines. The distribution takes a ‘‘propeller shape’’ tightly bounded by solid black lines γ_1 – γ_6 . All these bounds are fully characterized in Appendix F. The blue bounds show that \mathcal{E}_G is guaranteed to be positive whenever $\Delta I < -2\ln(5/4)$; the dotted lines cross at this turning point. Panel (b) illustrates what happens at higher dimensions, showcasing the $d_B = d_C = 6$ case. Compared to panel (a), the distribution is more concentrated around 0. This reflects the fact that both \mathcal{E}_G and ΔI asymptotically concentrate around their ensemble averages.

it comes to ergotropy transport. This is vividly seen in Fig. 2. Panels (a), (b), and (c) are histograms of \mathcal{E}_G calculated for a large sample of randomly sampled product states on randomly generated H_{BC} , acted upon by random U_{BC} . On panel (a), for B and C being two qubits, we see that \mathcal{E}_G never becomes positive, in accordance with Lemma 2. On panels (b) and (c), we see that, for higher-dimensional B and C , although \mathcal{E}_G is sometimes positive, its bulk becomes more and more negative as the system size grows. This aspect is numerically analyzed in more detail in Appendix C.

Figures 2(a)–(c) thus demonstrate that lack of correlations in the initial state is unfavorable for ergotropy transport. This motivates two questions: Which type of correlations matter the most? Is there a quantitative link between their strength and ergotropy gain \mathcal{E}_G ? Figures 2(d)–(f) shed some light on the first question. Each of these panels contains histograms of two ensembles of initial states: random (general) states of BC and random separable states of BC . As above, here H_{BC} and U_{BC} are also sampled randomly. We see that, in terms of ergotropy gain, separable states perform almost as well as all possible bipartite states, including the entangled ones. Thus, in the first approximation, the *type* of correlations does not play a significant role in the process of ergotropy transport. Note that we plot separable vs. general, and not separable vs. entangled, because efficiently characterizing the set of entangled states is impossible for $d_{BC} > 6$ [61]. However, it is possible to sample the separable set in arbitrary dimensions. In Appendix C, based on a pure-state decomposition of separable states from Ref. [62], we construct an efficient algorithm of generat-

ing random separable states that reasonably uniformly cover the whole separable set.

Now, having determined that the *type* of correlations has only a limited impact on the quality of transport, we are ready to answer the second question. To do so, we use the standard quantifier of “general” correlations—the quantum mutual information [63]: $I(\rho_{BC}) = S(\rho_B) + S(\rho_C) - S(\rho_{BC})$. Since the ergotropy gain is given by the change in the ergotropic gap [see Eq. (8)], we will compare \mathcal{E}_G with the *change* in the mutual information: $\Delta I = I(\tilde{\rho}_{BC}) - I(\rho_{BC})$ during the transport. In view of the unitary invariance of von Neumann entropy, we have

$$\Delta I = S(\tilde{\rho}_B) + S(\tilde{\rho}_C) - S(\rho_B) - S(\rho_C). \quad (9)$$

To reveal how the two quantities are related, we, as above, randomly sample a large ensemble of ρ_{BC} , H_{BC} , and U_{BC} , and plot ΔI against \mathcal{E}_G . This is done in Fig. 3, where 2×2 [panel (a)] and 6×6 [panel (b)] dimensional cases are depicted. For the two qubits, it reveals a propeller-like shape the axis of which passes through the center of the coordinates. The width of the distribution is significant, therefore there is no deterministic relation between ΔI and \mathcal{E}_G .

In higher dimensions, the ranges of ΔI and \mathcal{E}_G shrink, as is evidenced by Fig. 3(b). In Appendix D, we show that this phenomenon is general, by proving Levy-type measure-concentration bounds [64] for both \mathcal{E}_G and ΔI considered as functions of the initial state ρ_{BC} . There, and everywhere in this paper, we sample the states from the Hilbert–Schmidt measure. Our concentration bounds establish that the widths of the distributions of ΔI and \mathcal{E}_G decrease polynomially with d_B and d_C . In addition to that, as we numerically demonstrate in Appendix E, the relation between ΔI and \mathcal{E}_G becomes increasingly “deterministic”—for a given ΔI , the dispersion of possible \mathcal{E}_G ’s decreases with increasing dimensions, even adjusted for the shrinkage due to concentration.

The concentration of ΔI and \mathcal{E}_G means that, on the one hand, tailoring initial states and transfer unitaries such that ergotropy gain is significant becomes more increasingly complex as the dimensions grow higher. On the other hand, generic transport is robust in that both losses (and gains) are severely restricted.

Multiple transports and channel reusability.—As we saw above, correlations generically endow the initial state of BC with a positive ergotropic gap $\delta_{BC}^{\mathcal{E}}$, allowing one to avoid losses during transport. As Eq. (8) shows, each time $\mathcal{E}_G > 0$, this resource gets used up by that exact amount. While for a single transport having the largest \mathcal{E}_G is better, the situation changes when one wishes to perform multiple transports.

The latter is arguably the most relevant practical scenario, where our setup is a wire through which third parties send ergotropy to fourth parties, aiming for the highest number of lossless transports. Thus, having \mathcal{E}_G *positive but small* would be desirable, so that the initial supply of $\delta_{BC}^{\mathcal{E}}$ is consumed slowly. In this scenario, a key

quantity is the total amount of ergotropy, $\mathcal{E}_{\text{tot}}^+$, that one can losslessly transport through the channel in multiple iterations. Labelling transport iterations by the index ι , we can write

$$\mathcal{E}_{\text{tot}}^+ := \sum_{\iota; \mathcal{E}_G^{(\iota)} \geq 0} [\mathcal{E}(\tilde{\rho}_C^{(\iota)}) - \mathcal{E}(\rho_C^{(\iota)})]. \quad (10)$$

A paradigmatic protocol realizing this scenario is as follows. The system starts locally empty: both $\rho_B^{(0)}$ and $\rho_C^{(0)}$ are passive ($\rho_{BC}^{(0)}$ does not have to be uncorrelated). Then, a “charging” unitary U_{ch} acts locally on B , injecting some ergotropy into it. Next, an energy-conserving U_{BC} is performed on the total system, transporting ergotropy from B to C . Finally, a “draining” unitary U_{dr} acts locally on C , extracting (part of) its ergotropy. This comprises a full “transport cycle” of the channel, and is realized by the unitary operation

$$U_{\text{cyc}} = (\mathbb{1}_B \otimes U_{\text{dr}}) U_{BC} (U_{\text{ch}} \otimes \mathbb{1}_C). \quad (11)$$

Since the ergotropic gap depends only on the local and global spectra of the state [see Eq. (7)], U_{ch} and U_{dr} do not affect \mathcal{E}_G , only U_{BC} does. Thus, the ergotopic gap $\delta^{(0)} := \delta_{BC}^{\mathcal{E}}(\rho_{BC}^{(0)})$ of the initial “locally empty” state is the resource that will fuel the gainfulness of the transport, and it will be consumed over time.

For a transparent exemplification of this situation, we again turn to qubits and take $\rho_{BC}^{(0)} = |0\rangle_B\langle 0| \otimes |0\rangle_C\langle 0|$, $U_{\text{ch}} = U_{\text{dr}} = \sigma_X$, and $U_{BC} = \text{SWAP}$, where σ_X is the Pauli- X matrix. In this idealized scenario, the state returns to $|0\rangle_B\langle 0| \otimes |0\rangle_C\langle 0|$ after each transport cycle, and although $\mathcal{E}_G = 0$, an E amount of ergotropy is injected into B and the same E amount of ergotropy is extracted from C each time. Thus, this noiseless, idealized channel can be used infinitely many times to losslessly transport an infinite amount of ergotropy.

However, this behavior is not stable: a small deviation of U_{BC} from a swap will cause the transport to become lossy. Indeed, let us introduce a small error $\varepsilon \ll 1$ in the transport unitary:

$$U_{BC}^{(\varepsilon)} = \text{SWAP} + 2\nu_{BC}^{(\varepsilon)} \sin \frac{\varepsilon}{2}. \quad (12)$$

Here $\nu_{BC}^{(\varepsilon)} = \bar{\sigma}_Z \cos \frac{\varepsilon}{2} - \bar{\sigma}_X \sin \frac{\varepsilon}{2}$, where $\bar{\sigma}_X$ and $\bar{\sigma}_Z$ are the Pauli X and Z matrices in the subspace spanned by $|0_B 1_C\rangle$ and $|1_B 0_C\rangle$. Keeping $U_{\text{ch}} = U_{\text{dr}} = \sigma_X$, it is easy to calculate that, upon the ι ’th iteration of the transport cycle, the ergotropy gain will be $\mathcal{E}_G^{(\iota)} = -2E \sin(2\iota\varepsilon - \varepsilon) \sin \varepsilon$, which is negative for $1 \leq \iota \leq \pi/(2\varepsilon) + 1/2$.

To combat this lossiness, let us take an initial state with a positive ergotropic gap. For example, consider $\rho_{BC}^{(0)} = |\phi^{(0)}\rangle\langle\phi^{(0)}|$ with $|\phi^{(0)}\rangle = \cos \kappa |0_B 0_C\rangle + \sin \kappa |1_B 1_C\rangle$, where $0 < \kappa \leq \pi/4$ controls the initial ergotropic gap: $\delta^{(0)} = 2E \sin^2 \kappa > 0$. A simple calculation (detailed in Appendix G) shows that, in this case,

$$\mathcal{E}_G^{(\iota)} = 2E \sin(2\kappa + \varepsilon - 2\iota\varepsilon) \sin \varepsilon. \quad (13)$$

This quantity will be positive for the first $\lfloor \frac{\kappa}{\varepsilon} + \frac{1}{2} \rfloor$ iterations ($\lfloor x \rfloor$ is the floor function). For example, for $\varepsilon = 0.03$ and $\kappa = \pi/8$, the transport will be lossless during the first 13 iterations. As a result, $\mathcal{E}_{\text{tot}}^+ \approx 11.84E$ will be collected from C vis-à-vis only $\approx 11.54E$ amount of ergotropy that will be injected into B . Thus, a single slightly correlated state can be used to losslessly transport an order of magnitude more work ($\mathcal{E}_{\text{tot}}^+$) than it can store (E).

Lastly, we note that our multiple transfer setup is fundamentally different from that considered in Ref. [25]. Using our nomenclature, only uncorrelated, incoherent (diagonal) initial states are considered in Ref. [25], and a fresh battery is used upon each iteration.

Summary and outlook.—We introduced a paradigmatic setup of a quantum battery autonomously transporting ergotropy to a quantum device (consumption unit). We established that initial correlations between the battery and the device can significantly enhance the transport. Despite the channel being energy conserving, the device may get more ergotropy than the battery loses. Such gainful transport is counterintuitive as the natural expectation is that, when being transported, a useful resource should suffer dissipation.

We proved that, between two qubits, gainful transport is possible *only* if they are initially correlated. Whereas for higher-dimensional systems the correlation–ergotropy-gain relation becomes fuzzier, we showed that there, too, correlations maintain a central role.

We also established that both mutual information change and ergotropy gain concentrate around 0 with increasing dimensions. This implies that ergotropy transport between large systems is generically robust—while large gains are not to be expected, large losses are also unlikely.

Contributing to the robustness, we also observed that the *type* of correlations has only a secondary effect on the degree of gainfulness of transport. That said, as suggested by Fig. 2(d)–(f), entangled states have a slight advantage over separable ones. Understanding this subtle relationship is an interesting problem in its own right.

Lastly, we showed that initial correlations can have a long-lasting loss prevention effect when an imperfect channel repeatedly transports ergotropy through BC . If the channel has a small imperfection, even a modest amount of correlations between B and C can enable lossless transport of an order of magnitude more work than the storage capacity of B and C .

The framework developed here may serve as a stepping stone for further research into ergotropy transport under realistic conditions. A significant step would be accounting for environmental noise during transport, e.g., by considering non-unitary energy-conserving channels [37].

We thank Carsten Henkel and Marcin Łobejko for useful discussions. K.H. and J.A. are grateful for support from the University of Potsdam. J.A. gratefully acknowledges funding from the Deutsche Forschungsgemeinschaft (DFG, German Research Foundation) under Grants No. 384846402 and No. 513075417 and from the Engineering and Physical Sciences Research Council (EPSRC) (Grant No. EP/R045577/1) and thanks the Royal Society for support.

The code used to produce the data shown in Figs. 2–7 is available upon reasonable request to K.V.H., karen.hovhannisyan@uni-potsdam.de.

For the purpose of open access, the authors have applied a ‘Creative Commons Attribution’ (CC BY) licence to any Author Accepted Manuscript version arising from this submission.

[1] R. Alicki and M. Fannes, Entanglement boost for extractable work from ensembles of quantum batteries, *Phys. Rev. E* **87**, 042123 (2013).

[2] M. Perarnau-Llobet, K. V. Hovhannisyan, M. Huber, P. Skrzypczyk, N. Brunner, and A. Acín, Extractable work from correlations, *Phys. Rev. X* **5**, 041011 (2015).

[3] G. M. Andolina, M. Keck, A. Mari, M. Campisi, V. Giovannetti, and M. Polini, Extractable work, the role of correlations, and asymptotic freedom in quantum batteries, *Phys. Rev. Lett.* **122**, 047702 (2019).

[4] S. Tirone, R. Salvia, S. Chessa, and V. Giovannetti, Quantum work capacitances (2022), [arXiv:2211.02685 \[quant-ph\]](https://arxiv.org/abs/2211.02685).

[5] X. Yang, Y.-H. Yang, M. Alimuddin, R. Salvia, S.-M. Fei, L.-M. Zhao, S. Nimmrichter, and M.-X. Luo, Battery capacity of energy-storing quantum systems, *Phys. Rev. Lett.* **131**, 030402 (2023).

[6] K. V. Hovhannisyan, M. Perarnau-Llobet, M. Huber, and A. Acín, Entanglement generation is not necessary for optimal work extraction, *Phys. Rev. Lett.* **111**, 240401 (2008).

[7] F. C. Binder, S. Vinjanampathy, K. Modi, and J. Goold, Quantacell: powerful charging of quantum batteries, *New J. Phys.* **17**, 075015 (2015).

[8] F. Campaioli, F. A. Pollock, F. C. Binder, L. Céleri, J. Goold, S. Vinjanampathy, and K. Modi, Enhancing the charging power of quantum batteries, *Phys. Rev. Lett.* **118**, 150601 (2017).

[9] D. Ferraro, M. Campisi, G. M. Andolina, V. Pellegrini, and M. Polini, High-power collective charging of a solid-state quantum battery, *Phys. Rev. Lett.* **120**, 117702 (2018).

[10] J.-Y. Gyhm, D. Šafránek, and D. Rosa, Quantum charging advantage cannot be extensive without global operations, *Phys. Rev. Lett.* **128**, 140501 (2022).

[11] A. C. Santos, B. Çakmak, S. Campbell, and N. T. Zinner, Stable adiabatic quantum batteries, *Phys. Rev. E* **100**, 032107 (2019).

[12] D. Farina, G. M. Andolina, A. Mari, M. Polini, and V. Giovannetti, Charger-mediated energy transfer for

quantum batteries: An open-system approach, *Phys. Rev. B* **99**, 035421 (2019).

[13] F. Barra, Dissipative charging of a quantum battery, *Phys. Rev. Lett.* **122**, 210601 (2019).

[14] J. Liu, D. Segal, and G. Hanna, Loss-free excitonic quantum battery, *J. Phys. Chem. C* **123**, 18303 (2019).

[15] F. Pirmoradian and K. Mølmer, Aging of a quantum battery, *Phys. Rev. A* **100**, 043833 (2019).

[16] K. V. Hovhannisyan, F. Barra, and A. Imparato, Charging assisted by thermalization, *Phys. Rev. Res.* **2**, 033413 (2020).

[17] S. Gherardini, F. Campaioli, F. Caruso, and F. C. Binder, Stabilizing open quantum batteries by sequential measurements, *Phys. Rev. Res.* **2**, 013095 (2020).

[18] J. Q. Quach and W. J. Munro, Using dark states to charge and stabilize open quantum batteries, *Phys. Rev. Appl.* **14**, 024092 (2020).

[19] F. H. Kamin, F. T. Tabesh, S. Salimi, F. Kheirandish, and A. C. Santos, Non-Markovian effects on charging and self-discharging process of quantum batteries, *New J. Phys.* **22**, 083007 (2020).

[20] F. Barra, K. V. Hovhannisyan, and A. Imparato, Quantum batteries at the verge of a phase transition, *New J. Phys.* **24**, 015003 (2022).

[21] W.-L. Song, H.-B. Liu, B. Zhou, W.-L. Yang, and J.-H. An, Remote charging and degradation suppression for the quantum battery, *Phys. Rev. Lett.* **132**, 090401 (2024).

[22] F. Campaioli, S. Gherardini, J. Q. Quach, M. Polini, and G. M. Andolina, Colloquium: Quantum batteries (2023), [arXiv:2308.02277 \[quant-ph\]](https://arxiv.org/abs/2308.02277).

[23] J. Monsel, M. Fellous-Asiani, B. Huard, and A. Auffèves, The energetic cost of work extraction, *Phys. Rev. Lett.* **124**, 130601 (2020).

[24] S. Tirone, R. Salvia, and V. Giovannetti, Quantum energy lines and the optimal output ergotropy problem, *Phys. Rev. Lett.* **127**, 210601 (2021).

[25] M. Łobejko, P. Mazurek, and M. Horodecki, The asymptotic emergence of the second law for a repeated charging process (2022), [arXiv:2209.05339 \[quant-ph\]](https://arxiv.org/abs/2209.05339).

[26] D. Gelbwaser-Klimovsky, R. Alicki, and G. Kurizki, Work and energy gain of heat-pumped quantized amplifiers, *Europhys. Lett.* **103**, 60005 (2013).

[27] W. Niedenzu, D. Gelbwaser-Klimovsky, A. G. Kofman, and G. Kurizki, On the operation of machines powered by quantum non-thermal baths, *New J. Phys.* **18**, 083012 (2016).

[28] S. Seah, S. Nimmrichter, and V. Scarani, Work production of quantum rotor engines, *New J. Phys.* **20**, 043045 (2018).

[29] W. Niedenzu, M. Huber, and E. Boukobza, Concepts of work in autonomous quantum heat engines, *Quantum* **3**, 195 (2019).

[30] B. Çakmak, Ergotropy from coherences in an open quantum system, *Phys. Rev. E* **102**, 042111 (2020).

[31] S. Seah, M. Perarnau-Llobet, G. Haack, N. Brunner, and S. Nimmrichter, Quantum speed-up in collisional battery charging, *Phys. Rev. Lett.* **127**, 100601 (2021).

[32] A. E. Allahverdyan, R. Balian, and T. M. Nieuwenhuizen, Maximal work extraction from finite quantum systems, *Europhys. Lett.* **67**, 565 (2004).

[33] M. H. Partovi, Quantum thermodynamics, *Phys. Lett. A* **137**, 440 (1989).

[34] A. B. Brailovskii, V. L. Vaks, and V. V. Mityugov, Quantum models of relaxation, *Phys. Usp.* **39**, 745 (1996).

[35] D. Janzing, P. Wocjan, R. Zeier, R. Geiss, and T. Beth, Thermodynamic cost of reliability and low temperatures: Tightening Landauer's principle and the second law, *Int. J. Theor. Phys.* **39**, 2717 (2000).

[36] F. G. S. L. Brandão, M. Horodecki, J. Oppenheim, J. M. Renes, and R. W. Spekkens, Resource theory of quantum states out of thermal equilibrium, *Phys. Rev. Lett.* **111**, 250404 (2013).

[37] G. Chiribella and Y. Yang, Optimal quantum operations at zero energy cost, *Phys. Rev. A* **96**, 022327 (2017).

[38] J. Åberg, Catalytic coherence, *Phys. Rev. Lett.* **113**, 150402 (2014).

[39] J. A. Vaccaro, S. Croke, and S. M. Barnett, Is coherence catalytic?, *J. Phys. A* **51**, 414008.

[40] M. P. Woods, R. Silva, and J. Oppenheim, Autonomous quantum machines and finite-sized clocks, *Ann. Henri Poincaré* **20**, 125 (2019).

[41] M. H. Partovi, Entanglement versus stosszahlansatz: Disappearance of the thermodynamic arrow in a high-correlation environment, *Phys. Rev. E* **77**, 021110 (2008).

[42] D. Jennings and T. Rudolph, Entanglement and the thermodynamic arrow of time, *Phys. Rev. E* **81**, 061130 (2010).

[43] S. Jevtic, D. Jennings, and T. Rudolph, Maximally and minimally correlated states attainable within a closed evolving system, *Phys. Rev. Lett.* **108**, 110403 (2012).

[44] I. Henao and R. M. Serra, Role of quantum coherence in the thermodynamics of energy transfer, *Phys. Rev. E* **97**, 062105 (2018).

[45] G. M. Andolina, D. Farina, A. Mari, V. Pellegrini, V. Giovannetti, and M. Polini, Charger-mediated energy transfer in exactly solvable models for quantum batteries, *Phys. Rev. B* **98**, 205423 (2018).

[46] P. Lipka-Bartosik, G. F. Diotallevi, and P. Bakhshinezhad, Fundamental limits on anomalous energy flows in correlated quantum systems, *Phys. Rev. Lett.* **132**, 140402 (2024).

[47] M. Łobejko, P. Mazurek, and M. Horodecki, Thermodynamics of minimal coupling quantum heat engines, *Quantum* **4**, 375 (2020).

[48] T. Biswas, M. Łobejko, P. Mazurek, K. Jalowiecki, and M. Horodecki, Extraction of ergotropy: free energy bound and application to open cycle engines, *Quantum* **6**, 841 (2022).

[49] A. Mukherjee, A. Roy, S. S. Bhattacharya, and M. Banik, Presence of quantum correlations results in a nonvanishing ergotropic gap, *Phys. Rev. E* **93**, 052140 (2016).

[50] W. Pusz and S. L. Woronowicz, Passive states and KMS states for general quantum systems, *Commun. Math. Phys.* **58**, 273 (1978).

[51] A. Lenard, Thermodynamical proof of the Gibbs formula for elementary quantum systems, *J. Stat. Phys.* **19**, 575 (1978).

[52] Note that, whenever ρ or H have degenerate spectra, ρ^\downarrow will not be unique.

[53] M. Alimuddin, T. Guha, and P. Parashar, Bound on ergotropic gap for bipartite separable states, *Phys. Rev. A* **99**, 052320 (2019).

[54] K. Sen and U. Sen, Local passivity and entanglement in shared quantum batteries, *Phys. Rev. A* **104**, L030402 (2021).

[55] S. Puliyil, M. Banik, and M. Alimuddin, Thermodynamic signatures of genuinely multipartite entanglement, *Phys. Rev. Lett.* **129**, 070601 (2022).

[56] Here and throughout, $|i_B k_C\rangle \equiv |i\rangle_B \otimes |k\rangle_C$.

[57] Since entangled states always have nonzero quantum discord [65], this example may appear to contradict the claim of Ref. [49] that states with nonzero discord have positive ergotropic gap. However, there is no contradiction: in our case, the qubits have identical energy spectra, whereas the result of Ref. [49] applies only when the spectra are different.

[58] S. Bravyi, Requirements for compatibility between local and multipartite quantum states (2003), [arXiv:quant-ph/0301014 \[quant-ph\]](https://arxiv.org/abs/quant-ph/0301014).

[59] A. A. Klyachko, Quantum marginal problem and N-representability, *J. Phys. Conf. Ser.* **36**, 72 (2006).

[60] M. Christandl and G. Mitchison, The spectra of quantum states and the Kronecker coefficients of the symmetric group, *Commun. Math. Phys.* **261**, 789 (2005).

[61] R. Horodecki, P. Horodecki, M. Horodecki, and K. Horodecki, Quantum entanglement, *Rev. Mod. Phys.* **81**, 865 (2009).

[62] P. Horodecki, Separability criterion and inseparable mixed states with positive partial transposition, *Phys. Lett. A* **232**, 333 (1997).

[63] M. A. Nielsen and I. L. Chuang, *Quantum Computation and Quantum Information* (Cambridge University Press, Cambridge, 2010).

[64] V. D. Milman and G. Schechtman, *Asymptotic Theory of Finite Dimensional Normed Spaces*, Lecture Notes in Mathematics, Vol. 1200 (Springer, Berlin, 2001).

[65] B. Dakić, V. Vedral, and Č. Brukner, Necessary and sufficient condition for nonzero quantum discord, *Phys. Rev. Lett.* **105**, 190502 (2010).

[66] I. Bengtsson and K. Życzkowski, *Geometry of Quantum States: An Introduction to Quantum Entanglement* (Cambridge University Press, New York, 2006).

[67] Any pure state in a d -dimensional Hilbert space with some orthonormal basis $\{|k\rangle\}_{k=1}^d$ can be decomposed as $\sum_k c_k |k\rangle$, and the normalization condition means $\sum_k |c_k|^2 = 1$. This defines a $(2d-1)$ -dimensional sphere, and the Fubini–Study measure on pure states is simply the Haar measure on this sphere.

[68] J. Watrous, *The Theory of Quantum Information* (Cambridge University Press, Cambridge, 2018).

[69] V. Trávníček, K. Bartkiewicz, A. Černoch, and K. Lemr, Experimental measurement of the Hilbert–Schmidt distance between two-qubit states as a means for reducing the complexity of machine learning, *Phys. Rev. Lett.* **123**, 260501 (2019).

[70] N. Liu and P. Wittek, Vulnerability of quantum classification to adversarial perturbations, *Phys. Rev. A* **101**, 062331 (2020).

[71] M. Cerezo, A. Arrasmith, R. Babbush, S. C. Benjamin, S. Endo, K. Fujii, J. R. McClean, K. Mitarai, X. Yuan, L. Cincio, and P. J. Coles, Variational quantum algorithms, *Nat. Rev. Phys.* **3**, 625 (2021).

[72] V. V. Dodonov, O. V. Man'ko, V. I. Man'ko, and A. Wünsche, Hilbert–Schmidt distance and nonclassicality of states in quantum optics, *J. Mod. Opt.* **47**, 633 (2000).

[73] P. Pandya, O. Sakarya, and M. Wieśniak, Hilbert–Schmidt distance and entanglement witnessing, *Phys. Rev. A* **102**, 012409 (2020).

[74] D. Pérez-García, M. M. Wolf, D. Petz, and M. B. Ruskai, Contractivity of positive and trace-preserving maps under l_p norms, *J. Math. Phys.* **47**, 083506 (2006).

[75] M. Ozawa, Entanglement measures and the Hilbert–Schmidt distance, *Phys. Lett. A* **268**, 158 (2000).

[76] K. Życzkowski and H.-J. Sommers, Induced measures in the space of mixed quantum states, *J. Phys. A* **34**, 7111 (2001).

[77] F. Mezzadri, How to generate random matrices from the classical compact groups, *Not. Am. Math. Soc.* **54**, 592 (2007).

[78] D. Bures, An extension of Kakutani's theorem on infinite product measures to the tensor product of semifinite w^* -algebras, *Trans. Am. Math. Soc.* **135**, 199 (1969).

[79] A. Uhlmann, The “transition probability” in the state space of a $*$ -algebra, *Rep. Math. Phys.* **9**, 273 (1976).

[80] D. Petz, Monotone metrics on matrix spaces, *Linear Algebra Appl.* **244**, 81 (1996).

[81] S. L. Braunstein and C. M. Caves, Statistical distance and the geometry of quantum states, *Phys. Rev. Lett.* **72**, 3439 (1994).

[82] S.-i. Amari and H. Nagaoka, *Methods of Information Geometry* (Oxford University Press, New York, 2000).

[83] D. Petz and C. Sudár, Geometries of quantum states, *J. Math. Phys.* **37**, 2662 (1996).

[84] H.-J. Sommers and K. Życzkowski, Bures volume of the set of mixed quantum states, *J. Phys. A* **36**, 10083 (2003).

[85] P. B. Slater, Quantum Fisher–Bures information of two-level systems and a three-level extension, *J. Phys. A* **29**, L271 (1996).

[86] P. B. Slater, Comparative noninformativities of quantum priors based on monotone metrics, *Phys. Lett. A* **247**, 1 (1998).

[87] E. T. Jaynes, Prior probabilities, *IEEE Trans. Syst. Sci. Cybern.* **4**, 227 (1968).

[88] J. Dittmann, On the Riemannian metric on the space of density matrices, *Rep. Math. Phys.* **36**, 309 (1995).

[89] M. J. W. Hall, Random quantum correlations and density operator distributions, *Phys. Lett. A* **242**, 123 (1998).

[90] A. Sarkar and S. Kumar, Bures–Hall ensemble: spectral densities and average entropies, *J. Phys. A* **52**, 295203 (2019).

[91] P. B. Slater, Numerical and exact analyses of Bures and Hilbert–Schmidt separability and PPT probabilities, *Quantum Inf. Process.* **18**, 312 (2019).

[92] L. Wei and N. Witte, Quantum interpolating ensemble: Bi-orthogonal polynomials and average entropies, *Random Matrices: Theory Appl.* **12**, 2250055 (2023).

[93] A. R. Willms, Uniform sampling on the standard simplex, *Missouri J. Math. Sci.* **33**, 119 (2021).

[94] L. Devroye, *Non-Uniform Random Variate Generation* (Springer-Verlag, New York, 1986).

[95] A. Edelman and N. R. Rao, Random matrix theory, *Acta Numerica* **14**, 233– (2005).

[96] K. V. Hovhannisyan, R. P. A. Simon, and J. Anders, Continuity of ergotropy (2024), [arXiv:2406.0xxxx \[quant-ph\]](https://arxiv.org/abs/2406.0xxxx).

[97] P. Sekatski, J.-D. Bancal, X. Valcarce, E. Y.-Z. Tan, R. Renner, and N. Sangouard, Device-independent quantum key distribution from generalized CHSH inequalities, *Quantum* **5**, 444 (2021).

[98] G. T. Toussaint, Solving geometric problems with the rotating calipers, In: *Proc. IEEE MELECON* **83**, A10 (1983).

Appendix A: Proof of Lemma 2

To prove Lemma 2, let us without loss of generality set the energies of the ground states of B and C , $|0\rangle_B$ and $|0\rangle_C$, to zero. With this convention, the Hamiltonians write as $H_B = E_B |1\rangle_B\langle 1|$ and $H_C = E_C |1\rangle_C\langle 1|$.

There are two qualitatively different cases with regard to the structure of the energy-conserving unitary: $E_B \neq E_C$ and $E_B = E_C := E$. We treat them separately.

1. Case 1: $E_B \neq E_C$

In this case, $H_{BC} = H_B \otimes \mathbb{1}_C + \mathbb{1}_B \otimes H_C$ is nondegenerate, and therefore only operators that are diagonal in the energy eigenbasis can satisfy Eq. (2) in the main text. Thus, in the energy eigenbasis, energy-conserving unitaries are necessarily of the form

$$U_{BC} = \text{diag}(e^{i\phi_0}, e^{i\phi_1}, e^{i\phi_2}, e^{i\phi_3}). \quad (\text{A1})$$

It is now a simple exercise to check that the elements of the post-transfer state of B , $\tilde{\rho}_B = \text{Tr}_C [U_{BC}\rho_B \otimes \rho_C U_{BC}^\dagger]$, are

$$\begin{aligned} (\tilde{\rho}_B)_{00} &= (\rho_B)_{00}, \\ (\tilde{\rho}_B)_{01} &= (\rho_B)_{01} [(\rho_C)_{00} e^{i(\phi_0 - \phi_2)} + (\rho_C)_{11} e^{i(\phi_1 - \phi_3)}]. \end{aligned}$$

Due to the triangle inequality,

$$|(\rho_C)_{00} e^{i(\phi_0 - \phi_2)} + (\rho_C)_{11} e^{i(\phi_1 - \phi_3)}| \leq (\rho_C)_{00} + (\rho_C)_{11} = 1.$$

Therefore,

$$|(\tilde{\rho}_B)_{01}| \leq |(\rho_B)_{01}|. \quad (\text{A2})$$

Similarly, for $\tilde{\rho}_C = \text{Tr}_B [U_{BC}\rho_B \otimes \rho_C U_{BC}^\dagger]$, we have

$$\begin{aligned} (\tilde{\rho}_C)_{00} &= (\rho_C)_{00}, \\ (\tilde{\rho}_C)_{01} &= (\rho_C)_{01} [(\rho_B)_{00} e^{i(\phi_0 - \phi_1)} + (\rho_B)_{11} e^{i(\phi_2 - \phi_3)}], \end{aligned}$$

and

$$|(\tilde{\rho}_C)_{01}| \leq |(\rho_C)_{01}|. \quad (\text{A3})$$

Now, let us recall that the ergotropy of a qubit with the Hamiltonian $E|1\rangle\langle 1|$ is

$$\mathcal{E}(\rho) = E \left(\frac{1}{2} - \rho_{00} + \sqrt{\frac{1}{4} - \rho_{00}\rho_{11} + |\rho_{01}|^2} \right). \quad (\text{A4})$$

Thus, \mathcal{E} is a monotonically increasing function of $|\rho_{01}|$. Therefore, in view of Eqs. (A2) and (A3),

$$\mathcal{E}(\tilde{\rho}_B) \leq \mathcal{E}(\rho_B) \quad \text{and} \quad \mathcal{E}(\tilde{\rho}_C) \leq \mathcal{E}(\rho_C), \quad (\text{A5})$$

which in turn means that, according to its definition in Eq. (4) in the main text, the ergotropy gain $\mathcal{E}_G \leq 0$.

2. Case 2: $E_B = E_C := E$

Here the spectrum of H_{BC} is degenerate— $\text{Spec}(H_{BC}) = \{0, E, E, 2E\}$ —and hence there exist nontrivial energy-conserving unitaries. However, in this case, $\rho_B^\downarrow \otimes \rho_C^\downarrow$ is passive with respect to H_{BC} , and therefore $\delta_{BC}^\mathcal{E} = 0$ due to Eq. (7) in the main text. Indeed, denoting the eigenvalues of ρ_B and ρ_C by, respectively, $\lambda_0^B \geq \lambda_1^B$ and $\lambda_0^C \geq \lambda_1^C$, we have that

$$\rho_B^\downarrow \otimes \rho_C^\downarrow = \text{diag}(\lambda_0^B \lambda_0^C, \lambda_0^B \lambda_1^C, \lambda_1^B \lambda_0^C, \lambda_1^B \lambda_1^C)$$

in the energy eigenbasis. And since $\lambda_0^B \lambda_0^C \geq \lambda_0^B \lambda_1^C \geq \lambda_1^B \lambda_1^C$ and $\lambda_0^B \lambda_0^C \geq \lambda_1^B \lambda_0^C \geq \lambda_1^B \lambda_1^C$, this state is passive with respect to $H_{BC} = \text{diag}(0, E, E, 2E)$. Thus, due to Lemma 1, ergotropy transport by energy-conserving unitaries acting on product states cannot be gainful.

This concludes the proof of Lemma 2 in the main text.

Appendix B: Ergotropy transport and quantum marginal problem

In this section, we will show that our ergotropy transport problem is intimately connected to the problem of the compatibility of the spectra of local density matrices with the spectrum of the global density matrix, which is known as the “quantum marginal problem” (QMP) [59, 60].

For that, we first point out that, since the transport-performing operation U_{BC} is energy conserving [see Eq. (2) in the main text], $\rho_{BC}^\downarrow = \tilde{\rho}_{BC}^\downarrow$. Hence, due to Eq. (7) in the main text, the ergotropy gain in arbitrary Hilbert-space dimensions can be written as

$$\mathcal{E}_G = \sum_{k=0}^{d_B-1} E_k^B (\lambda_k^B - \tilde{\lambda}_k^B) + \sum_{k=0}^{d_C-1} E_k^C (\lambda_k^C - \tilde{\lambda}_k^C). \quad (\text{B1})$$

Here E_k^X ($X = B, C$) are the energy levels of the local Hamiltonian H_X ordered increasingly ($E_0^X \leq \dots \leq E_{d_X}^X$) and λ_k^X are the decreasingly ordered eigenvalues of the reduced density matrix ρ_X ($\lambda_0^X \geq \dots \geq \lambda_{d_X}^X$); the same applies to post-transport states $\tilde{\rho}_X$ and their eigenvalues $\tilde{\lambda}_k^X$.

Thus, the lossiness (or gainfulness) of ergotropy transport over an energy-conserving channel is determined solely by the initial and final spectra of the local states. Importantly, since transport is realized by a global unitary operation (U_{BC}), we have that $\text{Spec}(\rho_{BC}) = \text{Spec}(\tilde{\rho}_{BC})$. Therefore, the initial pair of local spectra ($\{\lambda_k^B\}_k$ and $\{\lambda_k^C\}_k$) and the final pair of local spectra ($\{\tilde{\lambda}_k^B\}_k$ and $\{\tilde{\lambda}_k^C\}_k$) must be compatible with the same global spectrum. So, both local spectra are related to each other by the fact that they must be a solution to the QMP for a given global density matrix spectrum.

This relation constitutes the connection of the QMP to the ergotropy transport problem. Below, to show the

strength of this connection, we prove Lemma 2 using the solution of the two-qubit QMP [58]. Furthermore, we show that the connection between the two problems goes both ways, by showing that a large subset of QMP inequalities derived in Ref. [59] can be obtained from the simple fact that the ergotropic gap is nonnegative.

1. From QMP to Lemma 2

As discussed in Appendix A, for two qubits we can set $E_0^B = E_0^C = 0$ without loss of generality, and to have nontrivial global-energy-conserving transport, $E_1^B = E_1^C = E$ must hold. In this energetic configuration, Eq. (B1) reduces to

$$\mathcal{E}_G = E(\lambda_1^B + \lambda_1^C - \tilde{\lambda}_1^B - \tilde{\lambda}_1^C). \quad (\text{B2})$$

Thus, lossy transport (i.e., $\mathcal{E}_G \leq 0$) is equivalent to

$$\lambda_1^B + \lambda_1^C \leq \tilde{\lambda}_1^B + \tilde{\lambda}_1^C. \quad (\text{B3})$$

Now, the solution of the QMP for two qubits (say, B and C) [58] is as follows. The local states ρ_B and ρ_C with spectra $\{\lambda_0^B \geq \lambda_1^B\}$ and $\{\lambda_0^C \geq \lambda_1^C\}$ can be the marginals of a global state ρ_{BC} with the spectrum $\{\lambda_0^{BC} \geq \lambda_1^{BC} \geq \lambda_2^{BC} \geq \lambda_3^{BC}\}$ only if

$$\lambda_1^B \geq \lambda_2^{BC} + \lambda_3^{BC}, \quad (\text{B4})$$

$$\lambda_1^C \geq \lambda_2^{BC} + \lambda_3^{BC}, \quad (\text{B5})$$

$$\lambda_1^B + \lambda_1^C \geq \lambda_1^{BC} + \lambda_2^{BC} + 2\lambda_3^{BC}, \quad (\text{B6})$$

$$|\lambda_1^B - \lambda_1^C| \leq \min\{\lambda_0^{BC} - \lambda_2^{BC}, \lambda_1^{BC} - \lambda_3^{BC}\}. \quad (\text{B7})$$

In the setting of Lemma 2, $\rho_{BC} = \rho_B \otimes \rho_C$, and therefore

$$\begin{aligned} \text{Spec}(\rho_{BC}) &= \text{Spec}(\tilde{\rho}_{BC}) \\ &= \{\lambda_0^B \lambda_0^C, \lambda_0^B \lambda_1^C, \lambda_1^B \lambda_0^C, \lambda_1^B \lambda_1^C\}. \end{aligned} \quad (\text{B8})$$

We immediately see that, with the above ordering convention, $\lambda_0^{BC} = \lambda_0^B \lambda_0^C$ and $\lambda_3^{BC} = \lambda_1^B \lambda_1^C$. For λ_1^{BC} and λ_2^{BC} , we have two options: either $\lambda_1^{BC} = \lambda_0^B \lambda_1^C$ and $\lambda_2^{BC} = \lambda_1^B \lambda_0^C$ or $\lambda_1^{BC} = \lambda_1^B \lambda_0^C$ and $\lambda_2^{BC} = \lambda_0^B \lambda_1^C$. In any case, we have that $\lambda_1^{BC} + \lambda_2^{BC} = \lambda_0^B \lambda_1^C + \lambda_1^B \lambda_0^C$. Therefore, applying Eq. (B6) to post-transport spectra $\{\tilde{\lambda}_0^B \geq \tilde{\lambda}_1^B\}$ and $\{\tilde{\lambda}_0^C \geq \tilde{\lambda}_1^C\}$, we get

$$\begin{aligned} \tilde{\lambda}_1^B + \tilde{\lambda}_1^C &\geq \lambda_0^B \lambda_1^C + \lambda_1^B \lambda_0^C + 2\lambda_1^B \lambda_1^C \\ &= \lambda_1^B + \lambda_1^C, \end{aligned} \quad (\text{B9})$$

which proves Eq. (F13) and thus Lemma 2.

2. From nonnegative ergotropic gap to QMP

Let us now show that we can turn around part of the argumentation used in the previous subsection to provide

a simple proof for a general family of inequalities for the QMP that were previously obtained in Ref. [59] using rather sophisticated mathematical machinery.

Suppose we have a bipartite system BC such that $\text{Spec}(\rho_B) = \{\lambda_0^B \geq \dots \geq \lambda_{d_B}^B\}$, $\text{Spec}(\rho_C) = \{\lambda_0^C \geq \dots \geq \lambda_{d_C}^C\}$, and $\text{Spec}(\rho_{BC}) = \{\lambda_0^{BC} \geq \dots \geq \lambda_{d_{BC}}^{BC}\}$.

Now, for *any* Hamiltonian $H_{BC} = H_B \otimes \mathbb{1}_C + \mathbb{1}_B \otimes H_C$, we have that $\delta_{BC}^E \geq 0$. To write this explicitly, following the notation used in Eq. (B1), let E_k^B and E_k^C be the increasingly-ordered eigenvalues of, respectively, H_B and H_C . Also, let $(E^B + E^C)_k$ be the increasingly-ordered eigenvalues of H_{BC} (which is simply the set $\{E_k^B + E_j^C\}_{k=0}^{d_B-1},_{j=0}^{d_C-1}$, but reordered from smallest to largest). In this notation,

$$\begin{aligned} \delta_{BC}^E &= \sum_{k=0}^{d_B-1} E_k^B \lambda_k^B + \sum_{k=0}^{d_C-1} E_k^C \lambda_k^C \\ &\quad - \sum_{k=0}^{d_B d_C - 1} (E^B + E^C)_k \lambda_k^{BC}, \end{aligned} \quad (\text{B10})$$

and the fact that $\delta_{BC}^E \geq 0$, leads us to

$$\sum_{k=0}^{d_B-1} E_k^B \lambda_k^B + \sum_{k=0}^{d_C-1} E_k^C \lambda_k^C \geq \sum_{k=0}^{d_B d_C - 1} (E^B + E^C)_k \lambda_k^{BC}. \quad (\text{B11})$$

We emphasize that this inequality holds for *any* choice of $\{E_k^B\}_k$ and $\{E_k^C\}_k$. Since the choice of the “zero level” of energy is arbitrary, we can, without loss of generality, additionally set

$$\sum_{k=0}^{d_B-1} E_k^B = \sum_{k=0}^{d_C-1} E_k^C = 0.$$

The family of inequalities given by Eq. (B11) coincides with the subset of QMP inequalities in “Example 3.5.1” of Ref. [59]. While this family is strictly smaller than the full set of QMP inequalities (Theorem 3.4.1 of Ref. [59]), it does cover a lot of ground, especially in low dimensions. To see that, let us go to the case of two qubits. By choosing $H_B = E|1\rangle_B\langle 1|$ and $H_C = 0$, we obtain Eq. (B4). By choosing $H_B = 0$ and $H_C = E|1\rangle_C\langle 1|$, we obtain Eq. (B5). And by choosing $H_B = E|1\rangle_B\langle 1|$ and $H_C = E|1\rangle_C\langle 1|$, we obtain Eq. (B6). So, three out of four QMP inequalities for two qubits can be obtained from the nonnegativity of the ergotropic gap.

Appendix C: Details of our numerical simulations

All thermodynamic and information-theoretic quantities that we calculate in this paper are fully determined by the initial state ρ_{BC} , the local Hamiltonians H_B and H_C , and the energy-conserving transport unitary U_{BC} . Here we give a detailed exposition of how we sample

random states, Hamiltonians, and energy-conserving unitaries in our numerical simulations. Out of many possible ways to randomly sample these quantities, we aimed at those that would cover the relevant sets fully, be physically meaningful, and mathematically well-defined.

The high-level procedure we follow is: (1) Generate a random ρ_{BC} (sometimes with a condition on the correlations). (2) Independently from ρ_{BC} , generate a random H_{BC} of the form in Eq. (3) in the main text, with the condition that its spectrum has nontrivial degeneracies. (3) Generate a random energy-conserving transport unitary U_{BC} that operates in the degenerate eigensubspaces of H_{BC} . Obviously, the sampling in step (3) strongly depends on the particular outcome of the sampling in step (2).

1. Sampling initial states

There are two important desiderata that a sensible probability measure on the space of density matrices should satisfy. First of all, in order to be analytically and numerically tractable, we require it to be induced by a Riemannian metric so that the volume element is constructed intuitively and can be written explicitly. Second, for such a metric—let us call it \mathcal{D} —we require unitary invariance: $\mathcal{D}(U\rho U^\dagger, U\sigma U^\dagger) = \mathcal{D}(\rho, \sigma)$ for arbitrary states ρ and σ and unitary U . These requirements ensure that \mathcal{D} is Fubini–Study–adjusted [66]. Namely, on pure states, \mathcal{D} coincides with the Fubini–Study metric, since the latter is the only (up to a constant factor) unitarily invariant Riemannian metric on pure states [66]. As a result of unitary invariance, the measure induced by the Fubini–Study metric is uniform on pure states [67]. Conveniently, random states of the form $U|0\rangle$, where $|0\rangle$ is some arbitrarily chosen pure state and U is sampled from the Haar measure on the unitary group $U(d)$, are distributed according to the Fubini–Study measure [66].

Among infinitely many unitarily invariant Riemannian metrics on the manifold of quantum states [66], the Hilbert–Schmidt and Bures metrics stand out. The former, defined as

$$\mathcal{D}_{\text{HS}}(\rho, \sigma) = \sqrt{\text{Tr}[(\rho - \sigma)^2]}, \quad (\text{C1})$$

is the generalization of the standard Euclidean metric for vectors to matrices, and it is widely used in quantum information [63, 66, 68] and computing [69–71] since it is intuitive and efficiently computable. Although it does not have a direct operational meaning, it has been used to quantify coherence and entanglement [72, 73]. Moreover, it is contractive (or “monotone”) under the action of unital channels [74] (but not under more general completely positive trace-preserving maps [75]).

Crucially, the measure induced by the Hilbert–Schmidt metric is also natural and intuitive. Indeed, take two copies of the system (B and B') and draw random pure states $|\Psi\rangle$ in the joint d^2 -dimensional Hilbert space from the Fubini–Study measure. Then, the density matrices

$\text{Tr}_{B'}|\Psi\rangle\langle\Psi|$ will be distributed according to the Hilbert–Schmidt measure in the Hilbert space of B [76]. Numerically, a more efficient way of sampling random density matrices from the Hilbert–Schmidt measure is to sample a $d \times d$ random Ginibre matrix G and compute

$$\rho = \frac{GG^\dagger}{\text{Tr}(GG^\dagger)}. \quad (\text{C2})$$

As was proven in Ref. [76], the states ρ are indeed distributed according to the Hilbert–Schmidt measure. We remind the reader that the elements of random Ginibre matrices are independent, identically identically distributed Gaussian random variables with mean = 0 and variance = 1 [77].

The other prominent metric—the Bures metric—defined as [78] $\mathcal{D}_B(\rho, \sigma) = \sqrt{2 - 2\sqrt{F(\rho, \sigma)}}$, where $F(\rho, \sigma) = (\text{Tr} \sqrt{\rho^{1/2}\sigma\rho^{1/2}})^2$ is the Uhlmann fidelity [79], has additional desirable properties that the Hilbert–Schmidt metric does not have. Namely, \mathcal{D}_B is contractive under the action of completely positive trace-preserving maps [66, 80] and Fisher-adjusted [66, 81] (i.e., for diagonal states, it coincides with the Fisher information metric [82]). In fact, \mathcal{D}_B is the only unitarily invariant Riemannian metric that has these properties [66, 83, 84]. Due to these unique properties, the measure induced by the Bures metric is considered [84–86] to be the quantum analog of the Jeffreys prior [82, 87]. The latter is the least informative distribution in classical statistics [82, 87] under certain generic conditions. Thus, the Bures measure is “the most random” measure, and it is a natural choice for revealing *generic* properties of states.

Despite these desirable properties, the curvature of the manifold of states in Bures metric diverges as the points of rank change [66, 88]. Moreover, the Bures measure is skewed towards pure states as compared to the Hilbert–Schmidt measure [66, 76, 89]. Thus, while the Bures measure is more random than the Hilbert–Schmidt measure, the latter is smooth and overall more “flat” in terms of purity. At the same time, the two measures are not too different in that they produce similar results in several contexts [90–92].

In our analysis, we require the measure from which states are sampled to be as random as possible, while guaranteeing a fair representation for density matrices of all ranks. Given all of the above, we believe the Hilbert–Schmidt measure strikes a good balance in that it (i) is natural in the sense that it is merely a reduction of the Fubini–Study measure, (ii) is close to the maximally random (Bures) measure, (iii) produces a flatter distribution with respect to purity than the Bures measure.

Therefore, in our numerical simulations, whenever we need to generate a random state of BC without any restrictions, we simply sample a $d_{BC} \times d_{BC}$ random density matrix from the Hilbert–Schmidt measure using Eq. (C2). Whenever we need to generate an uncorrelated state of the form $\rho_B \otimes \rho_C$, we sample ρ_B and ρ_C independently, each from the Hilbert–Schmidt measure.

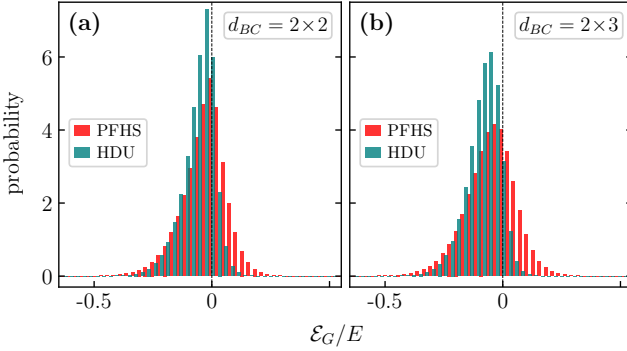


Figure 4. Comparing separable-state-sampling algorithms. Depicted are histograms of \mathcal{E}_G for randomly sampled separable initial states ρ_{BC} , Hamiltonians H_{BC} , and energy-conserving unitaries U_{BC} (similarly to Fig. 2). Each histogram is made up of 10^6 points. Panel (a) is for $d_{BC} = 2 \times 2$. The red histogram results from Peres-filtered Hilbert–Schmidt (PFHS) sampling of ρ_{BC} , whereas the green histogram results from the Horodecki-decomposed uniform (HDU) sampling algorithm. Panel (b) does the same as (a), but for $d_{BC} = 2 \times 3$. In both configurations, the distributions are fairly similar, although the one based on Eq. (C3) is slightly more concentrated. The color red PFHS sampling is chosen for consistency with Fig. 2, where, for 2×2 and 2×3 dimensions, separable states are sampled from PFHS.

The situation becomes more subtle when we need to generate random separable states of BC . Whenever $d_{BC} \leq 6$, doing so is relatively straightforward because it is easy to check whether a state is separable using the Peres criterion, i.e., partially transposing the state and checking if it is positive-semidefinite [61]. Thus, in order to generate a random separable state in $d_{BC} \leq 6$ dimensions, we can simply keep sampling random ρ_{BC} 's until we hit a separable state. Let us call this method Peres-filtered Hilbert–Schmidt (PFHS) sampling. This method is used to sample separable states in Figs. 2(d) and (e).

However, when $d_{BC} > 6$, checking whether a state is separable is unfeasible [61], so the mentioned technique becomes inapplicable. To go beyond this impasse, we use the fact, proven in Ref. [62], that any separable state of BC can be represented as a convex combination of at most d_{BC}^2 uncorrelated pure states. Thus, given that sampling from the Fubini–Study measure is the most sensible way of generating pure states, and it is what the Hilbert–Schmidt measure reduces to on pure states, we can generate random separable states as

$$\sum_{a=1}^{d_{BC}^2} p_a U_a^{(B)} |0\rangle_B \langle 0| U_a^{(B)\dagger} \otimes U_a^{(C)} |0\rangle_C \langle 0| U_a^{(C)\dagger}. \quad (\text{C3})$$

Here $|0\rangle_B$ and $|0\rangle_C$ are some arbitrarily chosen pure states of, respectively, B and C . Each random unitary $U_a^{(B)}$ is sampled from the Haar measure on the unitary group $U(d_B)$, and analogously for $U_a^{(C)}$. Haar-distributed unitary matrices can be generated by gen-

erating a full-rank Ginibre matrix and performing the Gram–Schmidt orthonormalization procedure to its rows (or columns) [77].

The coefficients $p_a \geq 0$ in Eq. (C3) form a $(d_{BC}^2 - 1)$ -dimensional simplex, $\sum_{a=1}^{d_{BC}^2} p_a = 1$, and they are also sampled randomly. Out of several intuitive ways of randomly sampling points from that simplex [93], we choose the uniform one. It is obtained by sampling $d_{BC}^2 - 1$ points κ_a from the uniform measure on $[0, 1]$, ordering them so that $0 \leq \tilde{\kappa}_1 \leq \dots \leq \tilde{\kappa}_{d_{BC}^2-1} \leq 1$, and taking $p_a = \tilde{\kappa}_a - \tilde{\kappa}_{a-1}$, with $\tilde{\kappa}_0 = 0$ and $\tilde{\kappa}_{d_{BC}^2} = 1$ [93, 94].

Now, since thus generated p_a 's cover the whole simplex and $U_a^{(B)} |0\rangle_B$'s and $U_a^{(C)} |0\rangle_C$'s cover all pure states of, respectively, B and C , the random separable states in Eq. (C3) cover all separable states of BC . Although we do not have a proof that this sampling is uniform on the manifold of separable states, it presumably achieves a reasonable degree of uniformity due to the fact that the distributions of p_a 's, $U_a^{(B)} |0\rangle_B$'s, $U_a^{(C)} |0\rangle_C$'s are as uniform as possible. We call this algorithm Horodecki-decomposed uniform (HDU) sampling. To benchmark it, we compare it with PFHS sampling in dimensions where the latter works reliably (i.e., $d_{BC} = 4$ and $d_{BC} = 6$). This is demonstrated in Fig. 4, where the histograms of the distributions of the ergotropy gain for these two separable-state-sampling algorithms are depicted. This plot shows that the difference between the two samplings is not big, meaning that HDU sampling generates sensible results. That said, as we can see in Fig. 4, it is more concentrated around the average, implying that, with respect to \mathcal{E}_G , it is slightly “less uniform” compared to PFHS sampling.

2. Sampling Hamiltonians

As with states, we want to sample Hamiltonians as generically as possible, while maintaining a fair representation for fringe cases. Most important fringe cases for Hamiltonians are those with degenerate spectra. Our strategy here is to start with maximal randomness and then gradually impose pertinent limitations.

Since any Hermitian operator can be a Hamiltonian, our starting point (before imposing limitations specific to our problem) is sampling Hermitian matrices as randomly as possible. To keep the possibilities as wide as possible, it is reasonable to require that all d^2 real parameters characterizing $d \times d$ Hermitian matrices to be statistically independent. Moreover, since there is no preferred basis in our problem, the probability measure should be invariant under unitary transformations. Remarkably, these two requirements unambiguously lead us to the Gaussian Unitary Ensemble (GUE) [95]. Moreover, sampling matrices H from the GUE is equivalent [95] to sampling

$$H = (G + G^\dagger)/2, \quad (\text{C4})$$

where G is a random Ginibre matrix.

Since in our case the total Hamiltonian is of the form $H_{BC} = H_B \otimes \mathbb{1}_C + \mathbb{1}_B \otimes H_C$ [see Eq. (3) in the main text], random Hamiltonian generation will consist of generating H_B and H_C separately. However, since we need H_{BC} to allow for nontrivial transport through energy-conserving unitaries, H_B and H_C must have at least one matching nonzero gap in their spectra. This matching condition means that H_B and H_C *cannot* be statistically independent.

Crucially, when H_B and H_C are sampled from the general GUE [Eq. (C4)], their eigenvalues can be any real numbers, and the subset of (H_B, H_C) pairs with matching gaps is of measure zero. Therefore, if one simply generates H_B and H_C , each according to Eq. (C4), then (H_B, H_C) pairs with matching gaps will almost never be encountered. To circumvent this problem, we coarse-grain the spectra of the Hamiltonians as follows. First, we generate a Hermitian matrix H using Eq. (C4). Then, we calculate its eigenvalues $E_0 \leq \dots \leq E_{d-1}$. Next, we choose the “grain” size of our coarse-graining, $\epsilon > 0$, and

if $E_k \in (\epsilon m - \epsilon/2, \epsilon m + \epsilon/2]$, $m \in \mathbb{Z}$, then $E_k \rightarrow \epsilon m$.

Thus, the coarse-grained spectrum, $\{\tilde{E}_0 \leq \dots \leq \tilde{E}_{d-1}\}$, is given by

$$\tilde{E}_k = \epsilon m_k, \quad \text{with} \quad m_k = \left\lceil \frac{E_k}{\epsilon} + \frac{1}{2} \right\rceil - 1, \quad (\text{C5})$$

where $\lceil x \rceil$ is the ceiling function. Finally, since the choice of the zero level of energy is arbitrary, we shift the spectrum so that $\tilde{E}_0 = 0$. All in all, this procedure leaves us with a coarse-grained Hamiltonian $\tilde{H} = \epsilon \text{diag}(0, m_1, \dots, m_{d-1})$, where $0 \leq m_1 \leq \dots \leq m_{d-1}$ are all integers. The degree of randomness of \tilde{H} has been limited only by the act of coarse-graining.

Now, coming up with $(\tilde{H}_B, \tilde{H}_C)$ pairs with matching coarse-grained gaps is numerically feasible: following the above procedure, we independently sample \tilde{H}_B and \tilde{H}_C (the grain size ϵ being the same in both cases). Then, we check if they have at least one matching nonzero gap. If not, we sample again.

The final aspect we need to account for, is setting the energy scale, or, equivalently, determining the dimensionless Hamiltonian. The above procedure generates a dimensionless matrix, and we need to make adjustments for it to be physically meaningful. To gain an intuition as to how to set the scale, let us consider three examples where that choice is obvious.

Example 1.—If $d_B = d_C = 2$, then the only Hamiltonian configuration allowing for nontrivial transport is $H_B = E |1\rangle_B \langle 1|$ and $H_C = E |1\rangle_C \langle 1|$. Here E sets the energy scale and the dimensionless Hamiltonians are simply $\text{diag}(0, 1)$.

Example 2.—If $d_B \geq 3$, \tilde{H}_B has equidistant levels, and C is simply a qubit, then the only configuration where transport is possible is $H_B = E \sum_k k |k\rangle_B \langle k|$ and

$H_C = Em |1\rangle_C \langle 1|$, with $m \leq d_B - 1$ a natural number. Obviously, here the dimensionless Hamiltonians are $\text{diag}(0, 1, 2, \dots, d_B - 1)$ and $\text{diag}(0, m)$, and E sets the energy scale.

Example 3.—If $d_B \geq 3$, $H_B = E \sum_{k=1}^{d_B-1} |k\rangle_B \langle k|$, and C is a qubit, then the only nontrivial possibility is that $H_C = E |1\rangle_C \langle 1|$. Here the dimensionless Hamiltonians are $\text{diag}(0, 1, 1, \dots)$ and $\text{diag}(0, 1)$, and, again, E sets the energy scale.

When the gaps of the Hamiltonian are not limited as in the examples above, they can be arbitrarily large. While this is certainly a theoretical possibility, in most real-life many-body systems the energy spectrum is limited, only slowly growing with the number of particles. Motivated by this observation and the three examples above, we will set the scale of the dimensionless Hamiltonian as follows. Step 1: Following the prescription described above, generate a random pair $(\tilde{H}_B, \tilde{H}_C)$ with at least one matching nonzero gap.

Step 2: Determine whose highest eigenvalue is larger. Suppose it is C , i.e., $\tilde{E}_{d_C-1} > \tilde{E}_{d_B-1}$.

Step 3: Determine M_C —the number of distinct eigenvalues of \tilde{H}_C (i.e., all degenerate eigenvalues count as one).

Step 4: Rescale the whole Hamiltonian, $\tilde{H}_B \otimes \mathbb{1}_C + \mathbb{1}_B \otimes \tilde{H}_C$, by $(M_C - 1)/\tilde{E}_{d_C-1}$. This will make sure that the maximal (dimensionless) energy of C is $M_C - 1$, and the rest will transform proportionally.

Step 5: If in Step 2 it was a tie, namely, $\tilde{E}_{d_C-1} = \tilde{E}_{d_B-1}$, then, for rescaling, choose the system with the largest number of distinct eigenvalues.

It is easy to check that, in the situations described by the examples above, this algorithm outputs the dimensionless Hamiltonians obtained in those examples. We use this Hamiltonian generation algorithm in our numerical simulations. In all our simulations, we set $\epsilon = 0.2$.

Of course, the randomness of this method is somewhat inhibited by coarse-graining, gap-matching, and rescaling (which are necessary to make the Hamiltonian appropriate for our problem and physically meaningful). Nonetheless, we believe that the vast range of configurations covered by these Hamiltonians is representative, and the sampling is reasonably fair in that it does not have any other biases than these three.

3. Sampling energy-conserving transport unitaries

Given a H_{BC} , sampling a fully random U_{BC} such that $[U_{BC}, H_{BC}] = 0$ is straightforward. Indeed, due to the commutation condition, U_{BC} can act nontrivially only in the degenerate eigensubspaces of H_{BC} . Let M_{BC} be the number of distinct eigenvalues $E_s^{(BC)}$ of H_{BC} , and $\{g_s\}_{s=1}^{M_{BC}}$ be the dimensions of the corresponding eigensubspaces. By definition, $\sum_s g_s = d_{BC}$, and due to the gap matching between B and C , at least one of g_s ’s will be ≥ 2 .

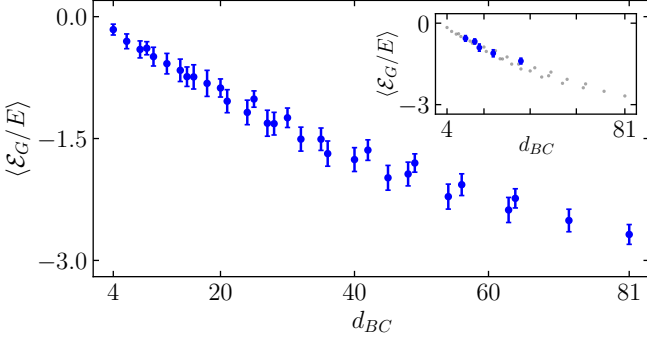


Figure 5. Ensemble-averaged dimensionless ergotropy gain, $\langle \mathcal{E}_G/E \rangle$, for initially uncorrelated B and C plotted against d_{BC} . The plot comprises 45 combinations of different dimensions $d_B = 2, \dots, 9$; $d_C = d_B, \dots, 9$. The “error bars” are given by the standard deviation of \mathcal{E}_G/E . We see that, as d_{BC} grows, uncorrelated states become increasingly lossy on average. Moreover, the standard deviation of \mathcal{E}_G/E remains significantly smaller than $|\langle \mathcal{E}_G/E \rangle|$, meaning that the likelihood of $\mathcal{E}_G > 0$ decreases with d_{BC} . For certain values of d_{BC} , there are more than one combinations of d_B and d_C such that $d_B d_C = d_{BC}$ (e.g., $12 = 2 \times 6 = 3 \times 4$). These “duplicate” configurations are not included in the main figure to avoid clutter. Rather, they are shown in the inset, along with $\langle \mathcal{E}_G/E \rangle$ for all d_{BC} (gray dots).

Then, for the Hilbert-space partitioning in which

$$H_{BC} = \bigoplus_{s=1}^{M_{BC}} E_s^{(BC)} \Pi_s^{(BC)},$$

where $\Pi_s^{(BC)}$ are the eigenprojectors of H_{BC} , we generate the random energy-conserving unitary as

$$U_{BC} = \bigoplus_{s=1}^{M_{BC}} U_s, \quad (\text{C6})$$

where, for each s , U_s is sampled according to the Haar measure from the unitary group $U(g_s)$.

4. Numerics for product initial states at higher dimensions

Here we will demonstrate the high-dimensional behaviour of \mathcal{E}_G when the initial state of BC is uncorrelated.

In Figs. 2(a)–(c), we observed that, in this case, the ensemble bulk of \mathcal{E}_G tends to become more and more negative as d_{BC} grows. Here we study this phenomenon more systematically, by simulating all possible system dimensions such that $d_{BC} \leq 81$. Figure 5 shows $\langle \mathcal{E}_G \rangle$ —the ensemble average of \mathcal{E}_G —as a function of d_{BC} . Each dot comes with a vertical bar corresponding to $\text{SD}(\mathcal{E}_G) = \sqrt{\langle \mathcal{E}_G^2 \rangle - \langle \mathcal{E}_G \rangle^2}$ —the standard deviation of \mathcal{E}_G over the ensemble. This plot clearly demonstrates that, generically, product states become increasingly lossy for er-

gotropy transport as the dimensions grow. This demonstrates that, while Lemma 2 does not hold in higher dimensions, correlations maintain their central role in increasing \mathcal{E}_G in that their lack generically leads to lossiness.

Thus, in order to have lossless or gainful ergotropy transport in higher dimensions, one has two choices. One either (i) starts uncorrelated but has to perform highly controlled operations on finely tuned Hamiltonians or (ii) uses correlated initial states and gains some “wiggle room” in the degree of control and fine tuning (see also Appendix G for more on that). Given that the first option is unrealistic at high dimensions, especially if one deals with many-body systems, the second option remains as the only viable choice.

Appendix D: Concentration of \mathcal{E}_G and ΔI in higher dimensions

Here we will use the Levy’s measure concentration bound [64] to show that the ergotropy gain and change of mutual information become concentrated in higher dimensions. As measure concentration bounds require Lipschitz continuity [64], we will invoke the ergotropy continuity result proven in Ref. [96].

First, let us formulate Levy’s inequality. Let $f(x)$ be a function mapping the $(N-1)$ -dimensional unit sphere to the real line (\mathbb{R}^1). Suppose $f(x)$ is Lipschitz continuous with respect to the Euclidean metric in the N -dimensional flat space (\mathbb{R}^N) in which the sphere is embedded. Now, if x is distributed according to the uniform Haar measure on the sphere, then [64]

$$\text{Prob} [|f(x) - \langle f \rangle| > \ell] \leq 3 e^{-\ell^2/\mathcal{B}_f^2}, \quad (\text{D1})$$

where the averaging $\langle f \rangle$ is over the Haar measure on the sphere and

$$\mathcal{B}_f = \frac{L_f}{\sqrt{\alpha N}}, \quad (\text{D2})$$

with L_f being the Lipschitz constant of f . The coefficient α is a universal constant; one can take $\alpha = 1/(25\pi)$ [68] (Theorem 7.37). The quantity \mathcal{B}_f controls the width of the distribution of f around its average. Intuitively, it can be thought of as an analogue of the standard deviation of f .

Now, it was proven in Ref. [96] that

$$|\mathcal{E}(\rho) - \mathcal{E}(\sigma)| \leq 2\|H\|_{\text{op}} \mathcal{D}_B(\rho, \sigma), \quad (\text{D3})$$

where $\|H\|_{\text{op}}$ is the operator norm of H , and in Refs. [96, 97] that

$$|S(\rho) - S(\sigma)| \leq L_S(d) \mathcal{D}_B(\rho, \sigma), \quad (\text{D4})$$

where

$$L_S(d) = \frac{2.322\pi}{2 \ln 2} \ln d. \quad (\text{D5})$$

To see the implications of these facts on our problem, let us fix the Hamiltonians H_B and H_C and pick an energy-conserving unitary U_{BC} . Then, we can easily see that both \mathcal{E}_G and ΔI are Lipschitz as functions of the initial state ρ_{BC} with respect to the Bures metric.

Indeed, starting with \mathcal{E}_G and using Eq. (4) in the main text, we can write

$$\begin{aligned} |\mathcal{E}_G(\rho_{BC}) - \mathcal{E}_G(\sigma_{BC})| &= |\mathcal{E}(\tilde{\rho}_B) + \mathcal{E}(\tilde{\rho}_C) - \mathcal{E}(\rho_B) \\ &\quad - \mathcal{E}(\rho_C) - \mathcal{E}(\tilde{\sigma}_B) - \mathcal{E}(\tilde{\sigma}_C) \\ &\quad + \mathcal{E}(\sigma_B) + \mathcal{E}(\sigma_C)| \\ &\leq |\mathcal{E}(\tilde{\rho}_B) - \mathcal{E}(\tilde{\sigma}_B)| \\ &\quad + |\mathcal{E}(\tilde{\rho}_C) - \mathcal{E}(\tilde{\sigma}_C)| \\ &\quad + |\mathcal{E}(\rho_B) - \mathcal{E}(\sigma_B)| \\ &\quad + |\mathcal{E}(\rho_C) - \mathcal{E}(\sigma_C)| \\ &\leq 2\|H_B\|_{\text{op}} \mathcal{D}_B(\tilde{\rho}_B, \tilde{\sigma}_B) \\ &\quad + 2\|H_B\|_{\text{op}} \mathcal{D}_B(\rho_B, \sigma_B) \\ &\quad + 2\|H_C\|_{\text{op}} \mathcal{D}_B(\tilde{\rho}_C, \tilde{\sigma}_C) \\ &\quad + 2\|H_C\|_{\text{op}} \mathcal{D}_B(\rho_C, \sigma_C), \end{aligned} \quad (\text{D6})$$

where in the last step we used Eq. (D3).

Furthermore, invoking the unitary invariance and contractivity of the Bures metric, we have that

$$\begin{aligned} \mathcal{D}_B(\tilde{\rho}_B, \tilde{\sigma}_B) &= \mathcal{D}_B(\text{Tr}_C[\tilde{\rho}_{BC}], \text{Tr}_C[\tilde{\sigma}_{BC}]) \\ &\leq \mathcal{D}_B(\tilde{\rho}_{BC}, \tilde{\sigma}_{BC}) \\ &= \mathcal{D}_B(\rho_{BC}, \sigma_{BC}), \end{aligned} \quad (\text{D7})$$

where in the last step we took into account that $\tilde{\rho}_{BC} = U_{BC}\rho_{BC}U_{BC}^\dagger$ and $\tilde{\sigma}_{BC} = U_{BC}\sigma_{BC}U_{BC}^\dagger$. Similarly,

$$\begin{aligned} \mathcal{D}_B(\rho_B, \sigma_B) &= \mathcal{D}_B(\text{Tr}_C[\rho_{BC}], \text{Tr}_C[\sigma_{BC}]) \\ &\leq \mathcal{D}_B(\rho_{BC}, \sigma_{BC}). \end{aligned} \quad (\text{D8})$$

Through identical steps, we also establish that

$$\begin{aligned} \mathcal{D}_B(\rho_C, \sigma_C) &\leq \mathcal{D}_B(\rho_{BC}, \sigma_{BC}), \\ \mathcal{D}_B(\tilde{\rho}_C, \tilde{\sigma}_C) &\leq \mathcal{D}_B(\rho_{BC}, \sigma_{BC}). \end{aligned} \quad (\text{D9})$$

All together, Eqs. (D6)–(D9) mean that \mathcal{E}_G is Lipschitz as a function of the initial state:

$$|\mathcal{E}_G(\rho_{BC}) - \mathcal{E}_G(\sigma_{BC})| \leq L_{\mathcal{E}_G} \mathcal{D}_B(\rho_{BC}, \sigma_{BC}), \quad (\text{D10})$$

with the Lipschitz constant

$$L_{\mathcal{E}_G} \leq 4(\|H_B\|_{\text{op}} + \|H_C\|_{\text{op}}). \quad (\text{D11})$$

Lastly, let $|\phi(\rho_{BC})\rangle$ be the purification of ρ_{BC} living in $\mathcal{H}_{BC} \otimes \mathcal{H}_{BC}$, where \mathcal{H}_{BC} is the Hilbert space of BC . By definition, $|\phi(\rho_{BC})\rangle$ be the purification of ρ_{BC} if $\rho_{BC} = \text{Tr}_{\text{copy of } \mathcal{H}_{BC}}[|\phi(\rho_{BC})\rangle \langle \phi(\rho_{BC})|]$. Then, it is easy to demonstrate (see, e.g., Ref. [96]) that $\mathcal{D}_B(\rho_{BC}, \sigma_{BC}) \leq \|\phi(\rho_{BC}) - \phi(\sigma_{BC})\|_2$, where $\|\cdot\|_2$

is the standard Euclidean metric in $\mathcal{H}_{BC} \otimes \mathcal{H}_{BC}$. With this, we also have that

$$|\mathcal{E}_G(\rho_{BC}) - \mathcal{E}_G(\sigma_{BC})| \leq L_{\mathcal{E}_G} \|\phi(\rho_{BC}) - \phi(\sigma_{BC})\|_2. \quad (\text{D12})$$

Turning to ΔI as a function of the initial state, we can upper-bound its Lipschitz constant by the exactly same reasoning as with \mathcal{E}_G . Indeed, using Eq. (9) in the main text and Eq. (D4), we write

$$\begin{aligned} |\Delta I(\rho_{BC}) - \Delta I(\sigma_{BC})| &= |S(\tilde{\rho}_B) + S(\tilde{\rho}_C) - S(\rho_B) \\ &\quad - S(\rho_C) - S(\tilde{\sigma}_B) - S(\tilde{\sigma}_C) \\ &\quad + S(\sigma_B) + S(\sigma_C)| \\ &\leq |S(\tilde{\rho}_B) - S(\tilde{\sigma}_B)| \\ &\quad + |S(\tilde{\rho}_C) - S(\tilde{\sigma}_C)| \\ &\quad + |S(\rho_B) - S(\sigma_B)| \\ &\quad + |S(\rho_C) - S(\sigma_C)| \\ &\leq L_S(d_B) \mathcal{D}_B(\tilde{\rho}_B, \tilde{\sigma}_B) \\ &\quad + L_S(d_B) \mathcal{D}_B(\rho_B, \sigma_B) \\ &\quad + L_S(d_C) \mathcal{D}_B(\tilde{\rho}_C, \tilde{\sigma}_C) \\ &\quad + L_S(d_C) \mathcal{D}_B(\rho_C, \sigma_C)]. \end{aligned} \quad (\text{D13})$$

Finally, using Eqs. (D7)–(D9), we conclude that ΔI is indeed Lipschitz as a function of the initial state:

$$\begin{aligned} |\Delta I(\rho_{BC}) - \Delta I(\sigma_{BC})| &\leq L_{\Delta I} \mathcal{D}_B(\rho_{BC}, \sigma_{BC}) \\ &\leq L_{\Delta I} \|\phi(\rho_{BC}) - \phi(\sigma_{BC})\|_2 \end{aligned} \quad (\text{D14})$$

with the Lipschitz constant

$$L_{\Delta I} \leq 2[L_S(d_B) + L_S(d_C)] = \frac{2.322\pi}{\ln 2} \ln d_{BC}. \quad (\text{D15})$$

As discussed in Appendix C 1, the initial states of BC are sampled from the Hilbert–Schmidt measure, which corresponds to sampling from the Fubini–Study measure on the pure states in $\mathcal{H}_{BC} \otimes \mathcal{H}_{BC}$. Now, let us pick an arbitrary basis $\{|\zeta\rangle\}_{\zeta=0}^{d_{BC}^2-1}$ in $\mathcal{H}_{BC} \otimes \mathcal{H}_{BC}$. Each pure state $|\phi\rangle$ can be decomposed as $|\phi\rangle = \sum_{\zeta} c(\phi)_{\zeta} |\zeta\rangle$, with $c(\phi)_{\zeta} = \langle \zeta | \phi \rangle$. The normalization condition yields

$$\sum_{\zeta=0}^{d_{BC}^2-1} (\text{Re}[c(\phi)_{\zeta}]^2 + \text{Im}[c(\phi)_{\zeta}]^2) = 1,$$

meaning that the set of pure states in $\mathcal{H}_{BC} \otimes \mathcal{H}_{BC}$ is equivalent to $\mathbb{S}^{2d_{BC}^2-1}$ —the $(2d_{BC}^2 - 1)$ -dimensional unit sphere embedded in $\mathbb{R}^{2d_{BC}^2}$. Moreover, the Euclidean norm in $\mathcal{H}_{BC} \otimes \mathcal{H}_{BC}$ is equivalent to the Euclidean norm in $\mathbb{R}^{2d_{BC}^2}$:

$$\|\phi\rangle - |\psi\rangle\|_2 = \|\overrightarrow{c(\phi)} - \overrightarrow{c(\psi)}\|_2,$$

where

$$\overrightarrow{c(\phi)} = \begin{bmatrix} \text{Re}[c(\phi)_0] \\ \text{Im}[c(\phi)_0] \\ \vdots \\ \text{Re}[c(\phi)_{d_{BC}^2-1}] \\ \text{Im}[c(\phi)_{d_{BC}^2-1}] \end{bmatrix}.$$

Most importantly, the Fubini–Study measure on the pure states in $\mathcal{H}_{BC} \otimes \mathcal{H}_{BC}$ is equivalent to the Haar measure on $\mathbb{S}^{2d_{BC}^2-1}$ [66].

Putting all this together, we conclude that, when ρ_{BC} is sampled from the Hilbert–Schmidt measure, the map $\mathcal{M}: \rho_{BC} \mapsto \overrightarrow{c(\phi(\rho_{BC}))}$ transforms $\mathcal{E}_G(\rho_{BC})$ into an $L_{\mathcal{E}_G}$ -Lipschitz function on $\mathbb{S}^{2d_{BC}^2-1}$, the argument of which is sampled uniformly, according to the Haar measure on $\mathbb{S}^{2d_{BC}^2-1}$. Similarly, the map \mathcal{M} transforms $\Delta I(\rho_{BC})$ to an $L_{\Delta I}$ -Lipschitz function on $\mathbb{S}^{2d_{BC}^2-1}$, the argument of which is sampled uniformly, according to the Haar measure on $\mathbb{S}^{2d_{BC}^2-1}$. Applying Levy’s inequality (D1) to both of these functions, and keeping in mind Eqs. (D11) and (D15), we thus find that

$$\text{Prob} [|\mathcal{E}_G - \langle \mathcal{E}_G \rangle| > \ell] \leq 3 e^{-\ell^2/\mathcal{B}_{\mathcal{E}_G}^2}, \quad (\text{D16})$$

with

$$\mathcal{B}_{\mathcal{E}_G} = \frac{\sqrt{25\pi} L_{\mathcal{E}_G}}{\sqrt{2d_{BC}^2}} \leq \frac{\sqrt{200\pi} (\|H_B\|_{\text{op}} + \|H_C\|_{\text{op}})}{d_{BC}}, \quad (\text{D17})$$

and

$$\text{Prob} [|\Delta I - \langle \Delta I \rangle| > \ell] \leq 3 e^{-\ell^2/\mathcal{B}_{\Delta I}^2}, \quad (\text{D18})$$

with

$$\mathcal{B}_{\Delta I} = \frac{\sqrt{25\pi} L_{\Delta I}}{\sqrt{2d_{BC}^2}} \leq \frac{65.951 \ln d_{BC}}{d_{BC}}. \quad (\text{D19})$$

Here the averages, $\langle \mathcal{E}_G \rangle$ and $\langle \Delta I \rangle$, are over the Hilbert–Schmidt measure in \mathcal{H}_{BC} . They are equal to the averages of the respective \mathcal{M} -transformed functions over the Haar measure on $\mathbb{S}^{2d_{BC}^2-1}$.

For in the simulations shown in Fig. 3(b) in the main text, we chose the dimensionless Hamiltonian to be such that $\|H\|_{\text{op}} = O(d)$; see Appendix C2. More precisely, it is easy to check that, there, $\|H_B\|_{\text{op}} + \|H_C\|_{\text{op}} \leq 2 \max\{d_B, d_C\}$. Thus, for the random Hamiltonian generation protocol of Appendix C2, that was used in Fig. 3(b),

$$\text{Prob} [|\mathcal{E}_G/E - \langle \mathcal{E}_G/E \rangle| > \ell] \leq 3 e^{-\ell^2/\tilde{\mathcal{B}}_{\mathcal{E}_G}^2}, \quad (\text{D20})$$

with

$$\tilde{\mathcal{B}}_{\mathcal{E}_G} < \frac{50.133 \max\{d_B, d_C\}}{d_B d_C}. \quad (\text{D21})$$

As already mentioned in Appendix C2, there are many ways to choose a dimensionless Hamiltonian. In those

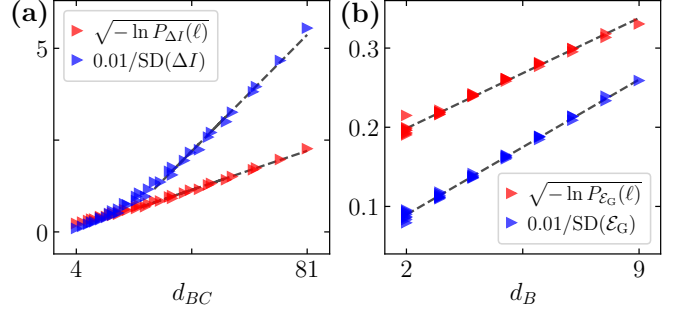


Figure 6. Here we plot the statistics of ΔI and \mathcal{E}_G against d_{BC} and d_B , in the sense of Eqs. (E3). As in Fig. 3, the states ρ_{BC} are sampled from the Hilbert–Schmidt measure, and H_{BC} and U_{BC} are sampled according to the protocols described in Appendix C. The sample size for each dot is 10^6 pints. Panel (a) is for ΔI , and the red line shows that, for larger d_{BC} ’s, $\sqrt{-\ln P_{\Delta I}(\ell)}$ scales linearly with d_{BC} . The blue line shows that $SD(\Delta I)^{-1}$ scales as d_{BC} , both confirming and giving additional meaning to Eq. (D19). Panel (b) does the same as Panel (a), but for \mathcal{E}_G/E vs d_B , again, confirming Eqs. (E3) and (D21). In both panels, $d_B \leq d_C$ run from 2 to 9 ($d_{BC} = 4, \dots, 81$), $\ell = 0.005$, and the 0.01 factor in front of $SD(\Delta I)^{-1}$ and $SD(\mathcal{E}_G)^{-1}$ is simply chosen to make the blue curves fit nicely with the red curves into the panels.

cases where B and C are known to be many-body systems with short-range interactions, the norm of their Hamiltonians would be proportional to the number of particles in those systems, namely, $\|H_B\|_{\text{op}} \propto \ln d_B$ and $\|H_C\|_{\text{op}} \propto \ln d_C$. Thus, for such systems, we would have $\tilde{\mathcal{B}}_{\mathcal{E}_G} = O\left(\frac{\ln d_{BC}}{d_{BC}}\right)$.

In any case, we see from Eqs. (D19) and (D21) that both distribution widths decay polynomially with d_B and d_C , which is what we see in Fig. 7.

Lastly, by the very construction of the ensemble, for each H_{BC} , the process $\rho_{BC} \rightarrow \tilde{\rho}_{BC}$ is equally likely as the $\tilde{\rho}_{BC} \rightarrow \rho_{BC}$ process. Therefore, $\langle \mathcal{E}_G \rangle = 0$ and $\langle \Delta I \rangle = 0$.

Appendix E: Numerics for higher-dimensional systems

As proven in Appendix D, when ρ_{BC} is sampled from the Hilbert–Schmidt measure, \mathcal{E}_G and ΔI concentrate around their ensemble-averages as d_B and d_C increase. This fact is also illustrated in Fig. (3) in the main text, where the ranges of \mathcal{E}_G and ΔI in panel (b) are significantly narrower than in panel (a). Here we numerically confirm the concentration bounds in Appendix D, and, on top of that, show that the relation between \mathcal{E}_G and ΔI becomes more deterministic even if we factor out the concentration phenomenon.

First, we confirm Eqs. (D18)–(D21). Denoting

$$P_{\Delta I}(\ell) := \text{Prob} [|\Delta I - \langle \Delta I \rangle| > \ell], \quad (\text{E1})$$

$$P_{\mathcal{E}_G}(\ell) := \text{Prob} [|\mathcal{E}_G/E - \langle \mathcal{E}_G/E \rangle| > \ell], \quad (\text{E2})$$

it is a simple exercise to check that, for large d_B , these bounds amount to

$$\begin{aligned}\sqrt{-\ln P_{\Delta I}(\ell)} &\propto \ell \frac{d_{BC}}{\ln d_{BC}}, \\ \sqrt{-\ln P_{\mathcal{E}_G}(\ell)} &\propto \ell d_B.\end{aligned}\quad (\text{E3})$$

In Fig. 6, we plot $P_{\Delta I}(\ell)$ and $P_{\mathcal{E}_G}(\ell)$ against, respectively, d_{BC} and d_B , and confirm that, at larger values of d_B and d_{BC} , the dependence is indeed linear, which conforms with Eqs. (E3); note that the presence of the logarithm becomes “invisible” for larger values of d_{BC} . Furthermore, given that \mathcal{B} is somewhat similar to the standard deviation, one could expect that the standard deviations of ΔI and \mathcal{E}_G/E , $\text{SD}(\Delta I)$ and $\text{SD}(\mathcal{E}_G)$, would scale with d_{BC} and d_B as, respectively, $\mathcal{B}_{\Delta I}$ and $\mathcal{B}_{\mathcal{E}_G}$. And indeed, as Fig. 6 shows, $\text{SD}(\Delta I)^{-1}$ and $\text{SD}(\mathcal{E}_G)^{-1}$ scale as, respectively, d_{BC} and d_B . Figure 6 thus corroborates the concentration bounds we obtained in Appendix D, additionally showing that the relevant quantities scale with d_B and d_{BC} in the same way as the bounds. It also confirms the intuition that the standard deviations behave like \mathcal{B} ’s.

The concentration bounds show that, as the dimensions increase, the relation between ΔI and \mathcal{E}_G becomes more and more deterministic simply due to the fact that ΔI and \mathcal{E}_G themselves become more deterministic as they concentrate around their respective averages. However, as we will argue here, this is not the whole story. Here we will argue that the relation between ΔI and \mathcal{E}_G becomes *even more deterministic* than is predicted by the concentration phenomenon.

To factor out the “shrinkage” due to concentration, we first pick an $N \gg 1$. Then, as in the simulations for Figs. 3 and 6, for each $d_B \times d_C$ configuration, we generate N random tuples $(\rho_{BC}, H_{BC}, U_{BC})$ from which we obtain an ensemble of N tuples $(\Delta I, \mathcal{E}_G/E)$. Now, for each $d_B \times d_C$, we take the observed $\max |\Delta I|$ and $\max |\mathcal{E}_G/E|$ over the corresponding ensemble and construct the rescaled ensemble consisting of N tuples $(\overline{\Delta I}, \overline{\mathcal{E}_G/E})$, where

$$\overline{\Delta I} = \frac{\Delta I}{\max |\Delta I|} \quad \text{and} \quad \overline{\mathcal{E}_G} = \frac{\mathcal{E}_G}{\max |\mathcal{E}_G/E|}. \quad (\text{E4})$$

Thus, for all d_B and d_C , $\overline{\Delta I} \in [-1, 1]$ and $\overline{\mathcal{E}_G} \in [-1, 1]$.

With the ranges of $\overline{\Delta I}$ and $\overline{\mathcal{E}_G}$ fixed, decrease in the dispersion in their relation with d_{BC} cannot be attributed to measure concentration and must therefore be a separate phenomenon. And reduction of dispersion is indeed what we observe at higher d_{BC} ’s. Indeed, for the same ensembles as in Fig. 6 (where $N = 10^6$ and there are 45 configurations of $d_B = 2, \dots, 9$ and $d_C = d_B, \dots, 9$), we made “propeller” plots of $(\overline{\Delta I}, \overline{\mathcal{E}_G})$. Two of these plots are shown in Panels (a) and (b) of Fig. 7. For each such plot, we first determine the convex hull of all the N points (using the built-in “ConvexHull” function of the Python library SciPy). Then, we use the method called “rotating

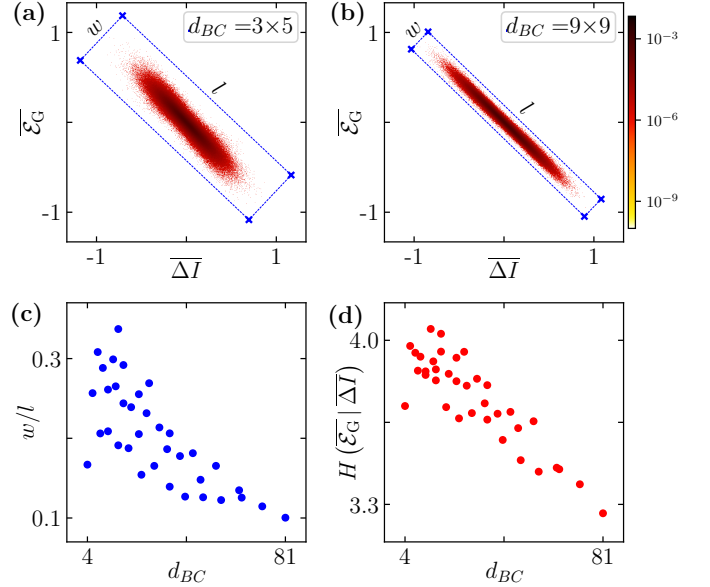


Figure 7. Here we demonstrate that the dispersion of the rescaled ergotropy gain, $\overline{\mathcal{E}_G}$ [see Eq. (E4)], with respect to the rescaled mutual information change, $\overline{\Delta I}$ decreases at higher dimensions. Panels (a) shows an ensemble of 10^6 tuples $(\overline{\Delta I}, \overline{\mathcal{E}_G})$ for $d_{BC} = 15$. Panel (b) shows the same, but for $d_{BC} = 81$. On each panel, the blue lines designate the rectangle with minimal area that contains all the points. The ratio w/l of the rectangle’s edges quantifies how disperse the dependence of $\overline{\mathcal{E}_G}$ on $\overline{\Delta I}$ is. Panel (c) shows w/l for $4 \leq d_{BC} \leq 81$. We see that the ratio becomes small at large d_{BC} ’s, meaning that $\overline{\mathcal{E}_G}$ becomes increasingly deterministic with respect to $\overline{\Delta I}$. Panel (d) shows the same trend, but now with the dispersion measured by $H(\overline{\mathcal{E}_G} | \overline{\Delta I})$ —the entropy of $\overline{\mathcal{E}_G}$ conditioned on $\overline{\Delta I}$. The smaller $H(\overline{\mathcal{E}_G} | \overline{\Delta I})$, the less the dispersion of $\overline{\mathcal{E}_G}$ with respect to $\overline{\Delta I}$.

calipers” [98] to find the rectangle with the smallest area that contains the whole complex hull. The ratio of the width w of the rectangle over its length l [see Figs. 7(a) and (b)] is a measure of the dispersion of the dependence of $\overline{\mathcal{E}_G}$ on $\overline{\Delta I}$. The corresponding rectangles are shown in Figs. 7(a) and (b), and we see that for $d_{BC} = 81$ the rectangle is significantly narrower than for $d_{BC} = 15$. The dependence of w/l on all values of d_{BC} is shown in Fig. 7(c), where we see that w/l tends to decrease as d_{BC} becomes large.

Another way of measuring how disperse $\overline{\mathcal{E}_G}$ is with respect to $\overline{\Delta I}$, is to consider $H(\overline{\mathcal{E}_G} | \overline{\Delta I})$ —the entropy of the random variable $\overline{\mathcal{E}_G}$ conditioned on the random variable $\overline{\Delta I}$ (in this case, over our N -point ensemble). When $H(Y|X) = 0$, then X is simply a deterministic function of Y , and the larger the $H(Y|X)$, the less deterministic the relation between X and Y . For our ensembles, we calculate $H(\overline{\mathcal{E}_G} | \overline{\Delta I})$ by coarse-graining the data into histograms and using the formula $H(\overline{\mathcal{E}_G} | \overline{\Delta I}) = H(\overline{\mathcal{E}_G}, \overline{\Delta I}) - H(\overline{\Delta I})$, where $H(\cdot)$ is the Shannon entropy of the argument. The dependence of the resulting condi-

tional entropy as a function of d_{BC} is shown in Fig. 7(d). Here, too, we see a downward trend at high dimensions, once again showing that the relation between $\overline{\mathcal{E}_G}$ and $\overline{\Delta I}$ tends to become more deterministic.

Lastly, we note that our approach towards factoring out the concentration is not unique. Once could, for example, rescale the axes by the standard deviation, not by the maximal observed range. There also exist alternative entropy-based methods of assessing dispersion of one variable with respect to another.

Appendix F: Bounds on the ergotropy gain for two qubits

Here we refine the relationship between \mathcal{E}_G and ΔI when B and C are qubits. We do so by establishing how much ergotropy gain is possible for a given change in mutual information.

First of all, let us show that the range of ΔI is $[-\ln 4, \ln 4]$ and that of \mathcal{E}_G is $[-E, E]$. Indeed, from Eq. (9) in the main text and the fact that, for a qubit, $0 \leq S(\rho) \leq \ln 2$, we immediately see that $-2 \ln 2 \leq \Delta I \leq 2 \ln 2$. Next, Eq. (8) in the main text and the fact that ergotropic gap is a nonnegative quantity imply that

$$-\tilde{\delta}_{BC}^{\mathcal{E}} \leq \mathcal{E}_G \leq \delta_{BC}^{\mathcal{E}}. \quad (\text{F1})$$

Now, for two identical qubits, Eq. (7) in the main text yields

$$\delta_{BC}^{\mathcal{E}} = E[\lambda_1^B + \lambda_1^C - (\lambda_1^{BC} + \lambda_2^{BC} - 2\lambda_3^{BC})], \quad (\text{F2})$$

where, as in Appendix B, λ_i^X are the eigenvalues of ρ_X in decreasing order. And since λ_1^B is the smaller eigenvalue of ρ_B , $\lambda_1^B \leq 1/2$. Similarly, $\lambda_1^C \leq 1/2$. Thus, by Eq. (F18), $\delta_{BC}^{\mathcal{E}} \leq E$, and thus, by Eq. (F1), $-E \leq \mathcal{E}_G \leq E$.

The main result of this appendix is that, by a combination of analytical derivations and numerical calculations (detailed below), we established that \mathcal{E}_G is upper-bounded as

$$\frac{\mathcal{E}_G}{E} \leq \begin{cases} \gamma_1(\Delta I), & \Delta I \in [-\ln 4, -\ln 2], \\ \max\{\gamma_1(\Delta I), \gamma_2(\Delta I)\}, & \Delta I \in [-\ln 2, 0], \\ \max\{\gamma_2(\Delta I), \gamma_3(\Delta I)\}, & \Delta I \in [0, \ln 2], \\ \gamma_3(\Delta I), & \Delta I \in [\ln 2, \ln 4], \end{cases} \quad (\text{F3})$$

and lower-bounded as

$$\frac{\mathcal{E}_G}{E} \geq \begin{cases} \gamma_4(\Delta I), & \Delta I \in [-\ln 4, -\ln 2], \\ \min\{\gamma_4(\Delta I), \gamma_5(\Delta I)\}, & \Delta I \in [-\ln 2, 0], \\ \min\{\gamma_5(\Delta I), \gamma_6(\Delta I)\}, & \Delta I \in [0, \ln 2], \\ \gamma_6(\Delta I), & \Delta I \in [\ln 2, \ln 4]. \end{cases} \quad (\text{F4})$$

The bounding functions γ_i are defined as

$$\begin{aligned} \gamma_1(x) &= 2h_+^{-1}\left(\frac{\ln 4+x}{2}\right) - 1, & x \in [-\ln 4, 0], \\ \gamma_2(x) &= 2h_+^{-1}\left(\frac{\ln 2+x}{2}\right) - \frac{3}{2}, & x \in [-\ln 2, \ln 2], \\ \gamma_3(x) &= 2h_+^{-1}\left(\frac{x}{2}\right) - 2, & x \in [0, \ln 4], \end{aligned} \quad (\text{F5})$$

and

$$\begin{aligned} \gamma_4(x) &= 2 - 2h_+^{-1}\left(-\frac{x}{2}\right), & x \in [-\ln 4, 0], \\ \gamma_5(x) &= \frac{3}{2} - 2h_+^{-1}\left(\frac{\ln 2-x}{2}\right), & x \in [-\ln 2, \ln 2], \\ \gamma_6(x) &= 1 - 2h_+^{-1}\left(\frac{\ln 4-x}{2}\right), & x \in [0, \ln 4]. \end{aligned} \quad (\text{F6})$$

Here

$$h_+^{-1} : [0, \ln 2] \mapsto [\frac{1}{2}, 1]$$

is the monotonically decreasing branch of the inverse of the binary entropy function $h(x) = -x \ln x - (1-x) \ln(1-x)$, $x \in [0, 1]$.

The bounds γ_1 – γ_6 are shown in Fig. 3 in the main text. There, the lines designated by γ_1 , γ_3 , γ_4 and γ_6 represent the most extreme cases achievable for two-qubit pure states. Whereas γ_2 and γ_5 give bounds for mixed states with two eigenvalues being $1/2$ and two eigenvalues being 0 . Note that while each γ_i is a valid bound only in a limited domain of ΔI , when appropriately combined [as per Eqs. (F3) and (F4)], the resulting bound is exact and holds for the full range of ΔI .

To derive Eqs. (F5) and (F6), we will use the solution to the quantum marginal problem for two qubits, and we will establish the veracity of the bounds in Eqs. (F3) and (F4) numerically. The solution of the two-qubit marginal problem is summarized in Eqs. (B4)–(B7), and, for the largest local eigenvalues, it writes as

$$\begin{aligned} \lambda_0^B &\leq \lambda_0^{BC} + \lambda_1^{BC}, \\ \lambda_0^C &\leq \lambda_0^{BC} + \lambda_1^{BC}, \\ \lambda_0^B + \lambda_0^C &\leq 2\lambda_0^{BC} + \lambda_1^{BC} + \lambda_2^{BC}, \\ |\lambda_0^B - \lambda_0^C| &\leq \min\{\lambda_0^{BC} - \lambda_2^{BC}, \lambda_1^{BC} - \lambda_3^{BC}\}. \end{aligned} \quad (\text{F7})$$

To obtain the bounds, we will look at the two extreme cases of the last line in Eq. (F7). One extreme case are the pure states of BC with $\text{Spec}(\rho_{BC}) = \{1, 0, 0, 0\}$. The other extreme case are the mixed states of BC such that $\text{Spec}(\rho_{BC}) = \{0.5, 0.5, 0, 0\}$. The states with more mixed spectra— $\{1/3, 1/3, 1/3, 0\}$ and $\{1/4, 1/4, 1/4, 1/4\}$ —turn out to be noninformative when used as extreme cases, as they delimit narrow sets that do not bound the ΔI – \mathcal{E}_G relation.

We will first look at the pure case, i.e., when $\text{Spec}(\rho_{BC}) = \{1, 0, 0, 0\}$. Here Eq. (F7) simply yields $\lambda_0^B = \lambda_0^C \leq 1$. And since $\tilde{\delta}_{BC}$ is also pure, $\tilde{\lambda}_0^B = \tilde{\lambda}_0^C \leq 1$ holds as well. Therefore,

$$\frac{\mathcal{E}_G}{2E} = \tilde{\lambda}_0^B - \lambda_0^B, \quad (\text{F8})$$

$$\frac{\Delta I}{2} = h(\tilde{\lambda}_0^B) - h(\lambda_0^B), \quad (\text{F9})$$

which brings us to

$$\tilde{\lambda}_0^B = h_+^{-1}\left(\frac{\Delta I}{2} + h(\lambda_0^B)\right), \quad (\text{F10})$$

$$\lambda_0^B = h_+^{-1}\left(h(\tilde{\lambda}_0^B) - \frac{\Delta I}{2}\right). \quad (\text{F11})$$

Substituting Eq. (F10) into Eq. (F8), we get

$$\frac{\mathcal{E}_G}{2E} = h_+^{-1} \left(\frac{\Delta I}{2} + h(\lambda_0^B) \right) - \lambda_0^B. \quad (\text{F12})$$

To find out how \mathcal{E}_G changes with λ_0^B , let us look into its derivative with respect to it:

$$\frac{d}{d\lambda_0^B} \frac{\mathcal{E}_G}{2E} = \frac{h'(\lambda_0^B)}{h'(h_+^{-1}(\frac{\Delta I}{2} + h(\lambda_0^B)))} - 1. \quad (\text{F13})$$

Keeping in mind that h_+^{-1} is monotonically decreasing, and that, in $[\frac{1}{2}, 1]$, h and h' are also monotonically decreasing, we have that

$$\begin{aligned} h'(h_+^{-1}(\frac{\Delta I}{2} + h(\lambda_0^B))) &\leq h'(\lambda_0^B) \leq 0, \quad \text{for } \Delta I \leq 0, \\ 0 &\geq h'(h_+^{-1}(\frac{\Delta I}{2} + h(\lambda_0^B))) \geq h'(\lambda_0^B), \quad \text{for } \Delta I \geq 0. \end{aligned}$$

Thus, in view of Eq. (F13), for $\Delta I \leq 0$, \mathcal{E}_G decreases with λ_0^B , and therefore $\mathcal{E}_G(\lambda_0^B) \leq \mathcal{E}_G(\frac{1}{2})$. Whereas for $\Delta I \geq 0$, \mathcal{E}_G increases with λ_0^B , meaning that $\mathcal{E}_G(\lambda_0^B) \leq \mathcal{E}_G(1)$. Reading from Eq. (F12), we thus have

$$\begin{aligned} \mathcal{E}_G/E &\leq \gamma_1(\Delta I), \quad \text{for } \Delta I \leq 0, \\ \mathcal{E}_G/E &\leq \gamma_3(\Delta I), \quad \text{for } \Delta I \geq 0. \end{aligned} \quad (\text{F14})$$

An analogous argumentation applied to Eq. (F11) gives birth to the lower bounds

$$\begin{aligned} \mathcal{E}_G/E &\geq \gamma_4(\Delta I), \quad \text{for } \Delta I \leq 0, \\ \mathcal{E}_G/E &\geq \gamma_6(\Delta I), \quad \text{for } \Delta I \geq 0. \end{aligned} \quad (\text{F15})$$

The functions γ_i are defined in Eqs. (F5) and (F6).

Lets now discuss the case were $\text{Spec}(\rho_{BC}) = \{0.5, 0.5, 0, 0\}$. Here Eqs. (F7) yield

$$\lambda_0^B + \lambda_0^C \leq 3/2, \quad (\text{F16})$$

$$|\lambda_0^B - \lambda_0^C| \leq 1/2. \quad (\text{F17})$$

The last line gives two extreme cases: (1) $|\lambda_0^B - \lambda_0^C| = 0$ (i.e., $\lambda_0^B = \lambda_0^C$) or (2) $|\lambda_0^B - \lambda_0^C| = 1/2$. In view of the fact that λ_0 's are the largest eigenvalues, case (2) simply means that either $\lambda_0^B = \lambda_0^C + 1/2$ or $\lambda_0^C = \lambda_0^B + 1/2$, which in turn implies that either $\lambda_0^B = 1/2$ and $\lambda_0^C = 1$ or $\lambda_0^B = 1$ and $\lambda_0^C = 1/2$. Since U_{BC} preserves the spectrum of the global state, we have the same extreme cases for $\tilde{\lambda}_0^B$ and $\tilde{\lambda}_0^C$: (1) $\tilde{\lambda}_0^B = \tilde{\lambda}_0^C$ and (2) either $\tilde{\lambda}_0^B = 1$ and $\tilde{\lambda}_0^C = 1/2$ or $\tilde{\lambda}_0^B = 1/2$ and $\tilde{\lambda}_0^C = 1$.

Now, cases (1)+(1) are already covered by the analysis above and yield the bounds in Eqs. (F14) and (F15). Cases (2)+(2) simply yield $I(\rho_{BC}) = I(\tilde{\rho}_{BC}) = 0$ and $\mathcal{E}(\rho_B) + \mathcal{E}(\rho_C) = \mathcal{E}(\tilde{\rho}_B) + \mathcal{E}(\tilde{\rho}_C) = E$, which are trivial and uninformative. The remaining two combinations—cases (1)+(2) and (2)+(1)—provide two additional meaningful bounds. Let us take the (1)+(2) configuration. For it,

$$\frac{\mathcal{E}_G}{E} = 3/2 - 2\lambda_0^B, \quad (\text{F18})$$

$$\Delta I = \ln 2 - 2h(\lambda_0^B). \quad (\text{F19})$$

As above, we express λ_0^B through ΔI and substitute it into Eq. (F18), which gives us $\mathcal{E}_G/E = \gamma_5(\Delta I)$. However, since, due to Eq. (F16), $\lambda_0^B \leq 3/4$, we have that $\mathcal{E}_G \geq 0$ and $-\ln 2 \leq \Delta I \leq -\frac{3}{2} \ln \frac{4}{3}$. Nonetheless, since the domain of h_+^{-1} is $[0, \ln 2]$, the function $\gamma_5(\Delta I)$ is well-defined on the whole range of $[-\ln 2, \ln 2]$, and therefore we will take the full function

$$\mathcal{E}_G/E = \gamma_5(\Delta I), \quad \text{for } \Delta \in [-\ln 2, \ln 2] \quad (\text{F20})$$

as a boundary.

Analyzing the (2)+(1) configuration analogously, we arrive at the boundary function

$$\mathcal{E}_G/E = \gamma_2(\Delta I), \quad \text{for } \Delta \in [-\ln 2, \ln 2]. \quad (\text{F21})$$

The functions γ_2 and γ_5 are defined in Eqs. (F5) and (F6).

Lastly, let us establish linear upper and lower bounds on \mathcal{E}_G in terms of ΔI . As the upper bound, we take the steepest tangential to γ_1 that does not cross γ_2 and γ_3 . It turns out, that this line is also tangent to γ_2 and γ_3 . Similarly, as a lower bound on \mathcal{E}_G , we take the steepest tangential to γ_6 that does not cross γ_5 and γ_4 . This line, too, happens to be tangent to γ_5 and γ_4 . Moreover, the two lines are parallel to each other and to the “trend line” connecting the most extreme points of \mathcal{E}_G . These points are $\mathcal{E}_G/E = 1, \Delta I = -\ln 4$ and $\mathcal{E}_G/E = -1, \Delta I = \ln 4$, and thus the trend line connecting them is

$$\mathcal{E}_G = -\frac{\Delta I}{\ln 4}. \quad (\text{F22})$$

Let us now find the value of ΔI for which the tangential of γ_4 is parallel to the trend line; namely, the solution of $d\gamma_4/d(\Delta I) = -1/(\ln 4)$. This will give us the linear lower bound. Using the inverse function rule, we find that

$$\frac{d\gamma_4}{d(\Delta I)} = \frac{1}{h'(h_+^{-1}(-\Delta I/2))} = \frac{1}{\ln \left(\frac{1}{h_+^{-1}(-\Delta I/2)} - 1 \right)},$$

and equating it to $-1/(\ln 4)$ immediately yields $\Delta I = -2h(1/5)$. At this value of ΔI , γ_4 evaluates to $2/5$, and therefore the line serving as the linear lower bound is

$$-\frac{\Delta I}{\ln 4} - \left(\frac{h(1/5)}{\ln 2} - \frac{2}{5} \right).$$

The above steps for γ_5 and γ_6 yield this same line, which proves that it is tangential to the three γ 's. Thus,

$$\frac{\mathcal{E}_G}{E} \geq -\frac{\Delta I}{\ln 4} - \left(\frac{h(1/5)}{\ln 2} - \frac{2}{5} \right). \quad (\text{F23})$$

A similar calculation with γ_1 (and then γ_2 and γ_3) yields the upper bound

$$\frac{\mathcal{E}_G}{E} \leq -\frac{\Delta I}{\ln 4} + \left(\frac{h(1/5)}{\ln 2} - \frac{2}{5} \right). \quad (\text{F24})$$

Using the lower bound in Eq. (F23), we immediately find the minimum value of ΔI necessary to ensure that $\mathcal{E}_G \geq 0$:

$$\Delta I_{\mathcal{E}_G \geq 0} \leq 2 \ln \frac{4}{5}. \quad (\text{F25})$$

Appendix G: Reusing a correlated state for multiple transports

Here we will calculate the ergotropy gain, and other relevant quantities, during iterations of the transport cycle. As detailed in the main text, the initial state is $\rho_{BC}^{(0)} = |\phi_{BC}^{(0)}\rangle\langle\phi_{BC}^{(0)}|$, with

$$|\phi_{BC}^{(0)}\rangle = \cos\kappa |0_B 0_C\rangle + \sin\kappa |1_B 1_C\rangle, \quad (\text{G1})$$

and the transport unitary is

$$U_{BC}^{(\varepsilon)} = \text{SWAP} + 2\nu_{BC}^{(\varepsilon)} \sin \frac{\varepsilon}{2} = \begin{pmatrix} 1 & 0 & 0 & 0 \\ 0 & \sin \varepsilon & \cos \varepsilon & 0 \\ 0 & \cos \varepsilon & -\sin \varepsilon & 0 \\ 0 & 0 & 0 & 1 \end{pmatrix}.$$

The “error” $\varepsilon \ll 1$ and “correlation resource” $0 < \kappa < \pi/4$. With such κ ’s, the initial ergotropic gap is

$$\delta^{(0)} = 2E \sin^2 \kappa.$$

The unitary operation performing a full cycle is

$$U_{\text{cyc}}^{(\varepsilon)} = (\mathbb{1}_B \otimes U_{\text{dr}}) U_{BC}^{(\varepsilon)} (U_{\text{ch}} \otimes \mathbb{1}_C) = \begin{pmatrix} \cos(\varepsilon) & 0 & 0 & \sin(\varepsilon) \\ 0 & 0 & 1 & 0 \\ 0 & 1 & 0 & 0 \\ -\sin(\varepsilon) & 0 & 0 & \cos(\varepsilon) \end{pmatrix}. \quad (\text{G2})$$

Hence, repeating the full transport ι times is equivalent to applying

$$(U_{\text{cyc}}^{(\varepsilon)})^\iota = \begin{pmatrix} \cos(\iota\varepsilon) & 0 & 0 & \sin(\iota\varepsilon) \\ 0 & \frac{1+(-1)^\iota}{2} & \frac{1-(-1)^\iota}{2} & 0 \\ 0 & \frac{1-(-1)^\iota}{2} & \frac{1+(-1)^\iota}{2} & 0 \\ -\sin(\iota\varepsilon) & 0 & 0 & \cos(\iota\varepsilon) \end{pmatrix}$$

to $|\phi_{BC}^{(0)}\rangle$, which means that the state of BC at the beginning of $(\iota+1)$ ’th cycle is

$$|\phi_{BC}^{(\iota+1), \text{in}}\rangle = \cos(\kappa - \iota\varepsilon) |0_B 0_C\rangle + \sin(\kappa - \iota\varepsilon) |1_B 1_C\rangle.$$

In this state of BC , the reduced states of B and C are

$$\begin{aligned} \rho_B^{(\iota+1), \text{in}} &= |0\rangle_B\langle 0| - \sigma_Z \sin^2(\kappa - \iota\varepsilon), \\ \rho_C^{(\iota+1), \text{in}} &= |0\rangle_C\langle 0| - \sigma_Z \sin^2(\kappa - \iota\varepsilon), \end{aligned}$$

where σ_Z is the Pauli Z matrix. As long as

$$\iota \leq \frac{\kappa}{\varepsilon} + \frac{\pi}{4\varepsilon}, \quad (\text{G3})$$

both $\rho_B^{(\iota+1), \text{in}}$ and $\rho_C^{(\iota+1), \text{in}}$ are passive. Thus, once U_{ch} is applied on B ,

$$\mathcal{E}_{\text{injected via } B}^{(\iota+1)} = E \cos(2\kappa - 2\iota\varepsilon) \quad (\text{G4})$$

amount of ergotropy is injected into the system via B , and the pre-transport state BC becomes

$$|\phi_{BC}^{(\iota+1)}\rangle = \cos(\kappa - \iota\varepsilon) |1_B 0_C\rangle + \sin(\kappa - \iota\varepsilon) |0_B 1_C\rangle.$$

So, the pre-transport reduced states are

$$\begin{aligned} \rho_B^{(\iota+1)} &= |0\rangle_B\langle 0| - \sigma_Z \cos^2(\kappa - \iota\varepsilon), \\ \rho_C^{(\iota+1)} &= |0\rangle_C\langle 0| - \sigma_Z \sin^2(\kappa - \iota\varepsilon), \end{aligned} \quad (\text{G5})$$

and

$$\begin{aligned} \mathcal{E}(\rho_B^{(\iota+1)}) &= E \cos(2\kappa - 2\iota\varepsilon), \\ \mathcal{E}(\rho_C^{(\iota+1)}) &= 0. \end{aligned} \quad (\text{G6})$$

Next, the application of the transport unitary $U_{BC}^{(\varepsilon)}$ leaves the system in the state

$$\begin{aligned} |\tilde{\phi}_{BC}^{(\iota+1)}\rangle &= \cos(\kappa - (\iota+1)\varepsilon) |0_B 1_C\rangle \\ &\quad + \sin(\kappa - (\iota+1)\varepsilon) |1_B 0_C\rangle, \end{aligned}$$

in which

$$\begin{aligned} \tilde{\rho}_B^{(\iota+1)} &= |0\rangle_B\langle 0| - \sigma_Z \sin^2(\kappa - (\iota+1)\varepsilon), \\ \tilde{\rho}_C^{(\iota+1)} &= |0\rangle_C\langle 0| - \sigma_Z \cos^2(\kappa - (\iota+1)\varepsilon). \end{aligned} \quad (\text{G7})$$

It is straightforward to check that, whenever

$$\iota + 1 \leq \frac{\kappa}{\varepsilon} + \frac{\pi}{4\varepsilon}, \quad (\text{G8})$$

the local ergotropies are

$$\begin{aligned} \mathcal{E}(\tilde{\rho}_B^{(\iota+1)}) &= 0, \\ \mathcal{E}(\tilde{\rho}_C^{(\iota+1)}) &= E \cos(2\kappa - 2(\iota+1)\varepsilon), \end{aligned} \quad (\text{G9})$$

and the optimal ergotropy-extracting unitary for $\tilde{\rho}_C^{(\iota+1)}$ is simply σ_X . Thus, the U_{dr} applied at the end of the cycle fully drains C , extracting

$$\mathcal{E}_{\text{extracted via } C}^{(\iota+1)} = \mathcal{E}(\tilde{\rho}_C^{(\iota+1)}) = E \cos(2\kappa - 2(\iota+1)\varepsilon). \quad (\text{G10})$$

We can now read off the ergotropy gain during the $(\iota+1)$ ’th cycle directly from Eqs. (G6) and (G9):

$$\mathcal{E}_G^{(\iota+1)} = 2E \sin(2\kappa - 2\iota\varepsilon - \varepsilon) \sin \varepsilon, \quad (\text{G11})$$

which coincides with Eq. (13) in the main text. From this expression, we immediately see that

$$\mathcal{E}_G^{(\iota)} \geq 0 \quad \text{for } 1 \leq \iota \leq \frac{\kappa}{\varepsilon} + \frac{1}{2}. \quad (\text{G12})$$

Note that the ι ’s in Eq. (G12) automatically satisfy the conditions in Eqs. (G3) and (G8). But the ranges of ι in Eqs. (G3) and (G8) go much beyond the range in Eq. (G12), meaning that, up to some finite value

of ι , BC can maintain a positive throughput, namely, $\mathcal{E}_{\text{extracted via } C}^{(\iota)} \geq 0$, even when $\mathcal{E}_G^{(\iota)} \leq 0$.

Finally, from Eqs. (G10) and (G6), we can write the total amount of ergotropy losslessly transported through

BC [see Eq. (10) in the main text] explicitly:

$$\mathcal{E}_{\text{tot}}^+ = E \sum_{\iota=1}^{\lfloor \frac{\kappa}{\varepsilon} + \frac{1}{2} \rfloor} \cos(2\kappa - 2\iota\varepsilon). \quad (\text{G13})$$